HRI-P-09-06-001

Two Higgs Doublet Type III Seesaw with μ-τ symmetry at LHC

Priyotosh Bandyopadhyay*, Sandhya Choubey†, Manimala Mitra‡

Harish–Chandra Research Institute,
Chhatnag Road, Jhunsi, 211019 Allahabad, India

September 3, 2018

Abstract

We propose a two Higgs doublet Type III seesaw model with μ-τ flavor symmetry. We add an additional SU(2) Higgs doublet and three SU(2) fermion triplets in our model. The presence of two Higgs doublets allows for natural explanation of small neutrino masses with triplet fermions in the 100 GeV mass range, without fine tuning of the Yukawa couplings to extremely small values. The triplet fermions couple to the gauge bosons and can be thus produced at the LHC. We study in detail the effective cross-sections for the production and subsequent decays of these heavy exotic fermions. We show for the first time that the μ-τ flavor symmetry in the low energy neutrino mass matrix results in mixing matrices for the neutral and charged heavy fermions that are not unity and which carry the flavor symmetry pattern. This flavor structure can be observed in the decays of the heavy fermions at LHC. The large Yukawa couplings in our model result in the decay of the heavy fermions into lighter leptons and Higgs with a decay rate which is about 10^{11} times larger than what is expected for the one Higgs Type III seesaw model with 100 GeV triplet fermions. The smallness of neutrino masses constrains the neutral Higgs mixing angle $\sin\alpha$ in our model in such a way that the heavy fermions decay into the lighter neutral CP even Higgs h^0, CP odd Higgs A^0 and the charged Higgs $H^\pm$, but almost never to the heavier neutral CP even Higgs H^0. The small value for $\sin\alpha$ also results in a very long lifetime for h^0. This displaced decay vertex should be visible at LHC. We provide an exhaustive list of collider signature channels for our model and identify those that have very large effective cross-sections at LHC and almost no standard model background.

*email: priyotosh@hri.res.in
†email: sandhya@hri.res.in
‡email: mmitra@hri.res.in

1 Introduction

Understanding of the flavor structure of the fermions has emerged as one of the most formidable problems in particle physics. While all fermions are expected to attain masses in the standard model through their Yukawa couplings with the standard Higgs doublet, it is not clear why the mass of the electron should be six order of magnitude smaller than that of the top quark. The extremely tiny neutrino masses pose a further challenge and demand an explanation. The "seesaw" mechanism [1] has been the most widely accepted method of explaining the smallness of the neutrino mass compared to that of the charge leptons. The seesaw mechanism was so named because the lightness of the standard neutrino is explained due to the heaviness of an additional particle beyond the standard model of particle physics. The new mass scale could be associated with a GUT scale, or in general with any intermediate mass scale. Being much heavier than the rest of the standard model particles, this additional field can be integrated out, giving a dimension five Majorana mass term for the neutrinos [2]. This mass term is inversely proportional to the mass of the heavy particle, and hence neutrinos become naturally light. There are three variants of the seesaw mechanism. These come from the fact that one can obtain the dimension five effective operator by integrating out either $SU(2)_L \times U(1)_Y$ (i) singlet fermions [1], or (ii) triplet scalars [3], or triplet fermions [4] (also [5]). The three variants are commonly known as Type I, Type II and Type III seesaw mechanism, respectively. While Type I and Type II scenarios have been extensively explored in the literature for a long time, focus has only recently shifted to the Type III seesaw mechanism, and a plethora of papers have appeared of late. While the possibility of gauged U(1) symmetry with fermion triplets was studied in [6], authors of [7] studied for the first time predictions for leptogenesis within the framework of Type III seesaw. A hybrid Type I+III seesaw framework is shown to result within a SU(5) GUT model in [8, 9], and within a left-right symmetric model with spontaneously broken parity in [10]. The effect of the additional fermions on the Higgs mass bounds was studied through renormalization group equations in [11], while the renormalization group evolution of the neutrino mass matrix within the Type III seesaw framework was performed in [12]. In [13] the authors work with just one extra heavy fermion triplet and generate the addition light neutrino masses at the loop level. The phenomenology of the Type III seesaw in lepton flavor violating processes was studied in great depths in [14, 15] and also recently in [16].

The most crucial feature concerning the Type III seesaw is the following. Since the additional heavy fermions belong to the adjoint representation of SU(2), they have gauge interactions. This makes it easier to produce them in collider experiments. With the LHC all set to take data, it is pertinent to check the viability of testing the seesaw models at colliders. The implications of the Type III seesaw at LHC was first studied in [17] and [18] in the context of a SU(5) GUT model. In the SU(5) model it is possible to naturally have the adjoint fermions in the 100 GeV to 1 TeV mass range, throwing up the possibility of observing them at LHC. The authors of these papers identified the dilepton channel with 4 jets as the signature of the triplet fermions. Subsequently, a lot of work has followed on testing Type III seesaw at LHC [19–21].

In the usual Type III (and also Type I) version of the seesaw models with one Higgs doublet, the neutrino mass is given by

$$m_\nu = -v^2 Y_\Sigma^T \frac{1}{M} Y_\Sigma \tag{1}$$

where, v is the Higgs Vacuum Expectation Value (VEV), M is the mass (matrix) of the adjoint fermions and Y_Σ is the Yukawa coupling (matrix) of these fermions with the standard model lepton doublets and Higgs. To predict neutrino masses ~ 0.1 eV without fine tuning the Yukawas, one requires that $M \sim 10^{14}$ GeV. On the other hand, an essential requisite of producing the heavy fermion triplet signatures at the LHC, is that they should not be heavier than a few hundred GeV. One can immediately see that if $M \sim 300$ GeV, then $m_\nu \sim 0.1$ eV demands that the Yukawa coupling $Y_\Sigma \sim 10^{-6}$. This in a way tentamounts to fine tuning of the Yukawas, and smothers out the very motivation for the seesaw mechanism – which was to explain the smallness of the neutrino mass without unnaturally reducing the Yukawa couplings.

In this paper, we propose a seesaw model with 300-800 GeV mass range triplet fermions, without any drastic reduction of the Yukawa couplings. We do that by introducing an additional Higgs doublet in our model. We impose a Z_2 symmetry which ensures that this extra Higgs doublet couples to only the exotic triplet fermions, while the standard Higgs couples to all other standard model particles [22]. As a result the smallness of the neutrino masses can be explained from the the smallness of the VEV of the second Higgs doublet, while all standard model fermions get their masses from the VEV of the standard Higgs. Therefore, we use the presence of two different VEVs in our model to explain the smallness of the neutrino masses compared to all others, without resorting to unnatural suppression of the neutrino Yukawa couplings. We show that these large Yukawas result in extremely fast decay rates for the heavy fermions in our model and hence have observational consequences for the heavy fermion phenomenology at LHC. We show how this can be used to distinguish our two Higgs doublet Type III seesaw model from the usual one Higgs doublet models.[1]

The presence of two Higgs doublets in our model also enhances the richness of the phenomenology at LHC. We have in our model two neutral physical scalar and one neutral physical pseudoscalar and a pair of charged scalars. We will work out in detail our Higgs mass spectrum by imposing constraints coming from the neutrino masses. We will show that due to these constraints, our Higgs mixing angle is very small and the Higgs behave in a very peculiar way and have collider signatures which are very different from the usual two Higgs doublet models in the market [23–27]. We will study this crucial link between neutrino and Higgs physics in our model and its implications for LHC in detail.

Another feature associated with neutrinos which has puzzled model builders is it unique mixing pattern. While all mixing angles are tiny in the quark sector, for the leptons we have observed two large and one small mixing angle. In its standard parametrization with

[1]The largeness of the Yukawa couplings (along with the smallness of the heavy fermion masses), also brings in larger non-unitarity and larger lepton flavor violation in our model, compared to the earlier Type III seesaw models. However, these are still well below the sensitivity of the current and upcoming future experiments.

mixing angles θ_{12}, θ_{23} and θ_{13} and phases δ (Dirac), α and β (Majorana), the neutrino mixing matrix is given as

$$U_{PMNS} = \begin{pmatrix} c_{12}\,c_{13} & s_{12}\,c_{13} & s_{13}\,e^{-i\delta} \\ -c_{23}\,s_{12} - s_{23}\,s_{13}\,c_{12}\,e^{i\delta} & c_{23}\,c_{12} - s_{23}\,s_{13}\,s_{12}\,e^{i\delta} & s_{23}\,c_{13} \\ s_{23}\,s_{12} - c_{23}\,s_{13}\,c_{12}\,e^{i\delta} & -s_{23}\,c_{12} - c_{23}\,s_{13}\,s_{12}\,e^{i\delta} & c_{23}\,c_{13} \end{pmatrix} \begin{pmatrix} 1 & 0 & \\ 0 & e^{i\alpha} & 0 \\ 0 & 0 & e^{i(\beta+\delta)} \end{pmatrix}. \quad (2)$$

In this parametrization, the mixing angle θ_{23} is observed to be very close to $\pi/4$, while θ_{13} has so far been seen to be consistent with zero. This indicates that there should be some underlying symmetry which drives one mixing angle to be maximal and another to be zero. The most simple way of generating this is by imposing a μ-τ exchange symmetry on the low energy neutrino mass matrix [28].

In this paper we will impose the μ-τ symmetry on the Yukawa couplings and the heavy fermion mass matrices. This leads to μ-τ symmetry in the light neutrino mass matrix and hence the correct predictions for the neutrino oscillation data. We discuss in detail the light as well as heavy neutrino mixing. We first provide general expressions for all mass eigenvalues and mixing matrices and then study the experimental consequences for our model. We show that due to the μ-τ symmetry, the mixing matrices of the heavy fermions turn out to be non-trivial. In particular, they are also μ-τ symmetric and hence much deviated from unity, even though we start with a real and diagonal Majorana mass matrix for the heavy triplets. This is a new result and we will show that this affects the flavor structure of the heavy fermion decays at colliders, which can be used to test μ-τ symmetry in neutrinos at LHC. We study in detail the collider phenomenology of this μ-τ symmetric model with three heavy fermion SU(2) triplets and two Higgs SU(2) doublets and give predictions for LHC.

The paper is organized as follows. In section 2, we present the lepton Yukawa part of the model within a general framework and give expressions for the masses and mixings of the charged and neutral components of both light as well as heavy leptons. In section 3, we present our μ-τ symmetric model and give specific forms for the mass and mixing parameters. We show that the mixing for heavy fermions is non-trivial and μ-τ symmetric. In section 4, we study the cross-section for the heavy fermion production and LHC, as a function of the fermion mass. In section 5, we study the decay rates of these heavy fermions into Higgs and gauge bosons. We compare and contrast our model against the usual Type III seesaw models with only one Higgs. We also show the consequences of non-trivial mixing of the heavy fermions on the flavor structure of their decays. In section 6, we discuss the decay rates and branching ratios of the Higgs decays. We probe issues on Higgs decays, which are specific and unique to our model. Section 7 is devoted to the discussion of displaced decay vertices as a result of the very long living h^0 in our model. In section 8, we list all possible final state particles and their corresponding collider signature channels which could be used to test our model. We calculate the effective cross-sections for all channels at LHC. We highlight some of the channels with very large effective cross-sections and discuss the standard model backgrounds. Finally, in section 9 we present our conclusions. Discussion of the scalar potential, the Higgs mass spectrum and the constraints from neutrino data on the Higgs sector is discussed in detail in Appendix A.

The lepton-Higgs coupling vertices are listed in Appendix B.1, the lepton-gauge coupling vertices are listed in Appendix B.2, and the quark-Higgs coupling vertices are listed in Appendix B.3.

2 Yukawa Couplings and Lepton Masses and Mixing

We add three extra SU(2) triplet fermions to our standard model particle content. These fermions belong to the adjoint representation of SU(2) and are assigned hypercharge $Y = 0$. This makes each of them self conjugate. We will denote their Cartesian components as[2]

$$\Psi'_i = \begin{pmatrix} \Sigma'^1_i \\ \Sigma'^2_i \\ \Sigma'^3_i \end{pmatrix}, \tag{3}$$

where $i = 1, 2, 3$ and $\Psi'_i = \Psi'^C_i$. In the compact 2×2 notation they will be represented in our convention as

$$\Sigma'_i = \frac{1}{\sqrt{2}} \sum_j \Sigma'^j_i \cdot \sigma_j, \tag{4}$$

where σ_j are the Pauli matrices. The right-handed component of this multiplet in the 2×2 notation is then given by

$$\Sigma'_{Ri} = \begin{pmatrix} \Sigma'^0_{Ri}/\sqrt{2} & \Sigma'^+_{Ri} \\ \Sigma'^-_{Ri} & -\Sigma'^0_{Ri}/\sqrt{2} \end{pmatrix}, \tag{5}$$

where

$$\Sigma'^{\pm}_{R\,i} = \frac{\Sigma'^1_{Ri} \mp i\Sigma'^2_{Ri}}{\sqrt{2}} \quad \text{and} \quad \Sigma'^0_{Ri} = \Sigma'^3_{Ri} \tag{6}$$

are the components of the triplet in the charge eigenbasis. The corresponding charge-conjugated multiplet will then be

$$\Sigma'^{\,C}_{R_i} = C\overline{\Sigma'_R}^T = \begin{pmatrix} \Sigma'^{0\;C}_{R_i}/\sqrt{2} & \Sigma'^{+\;C}_{R_i} \\ \Sigma'^{-\;C}_{Ri} & -\Sigma'^{0\;C}_{Ri}/\sqrt{2} \end{pmatrix}. \tag{7}$$

The object which transforms as the left-handed component of the Σ multiplet can then be written as

$$\tilde{\Sigma}'^C_{R_i} = i\sigma_2\, \Sigma'^{\,C}_{R_i}\, i\sigma_2 = \begin{pmatrix} \Sigma'^{0\;C}_{R_i}/\sqrt{2} & \Sigma'^{-\;C}_{R_i} \\ \Sigma'^{+\;C}_{Ri} & -\Sigma'^{0\;C}_{Ri}/\sqrt{2} \end{pmatrix}, \tag{8}$$

[2]Throughout this paper we denote particles in their weak eigenbasis by primed and mass eigenbasis by unprimed notation.

such that ${\Sigma'}_i = {\Sigma'}_{R_i} + \tilde{{\Sigma'}}^C_{R_i}$.

As discussed in the introduction, we include in our model a new SU(2) scalar doublet, Φ_2, in addition to the usual standard model doublet Φ_1. This new doublet couples only to the triplet fermions introduced above. The triplet fermions on the other hand are restricted to couple with only the new Φ_2 doublet and not with Φ_1. This can be ensured very easily by giving Z_2 charge of -1 to the triplet fermions Σ'_i and the scalar doublet Φ_2, and Z_2 charge $+1$ to all standard model particles[3]. The part of the Lagrangian responsible for the lepton masses can then be written as

$$-\mathcal{L}_Y = \left[Y_{l_{ij}} \overline{l'}_{R_i} \Phi_1^\dagger L'_j + Y_{\Sigma_{ij}} \tilde{\Phi}_2^\dagger \overline{\Sigma'}_{R_i} L'_j + h.c.\right] + \frac{1}{2} M_{ij}\, \mathrm{Tr}\left[\overline{\Sigma'}_{R_i} \tilde{{\Sigma'}}^C_{R_j} + h.c.\right], \tag{9}$$

where L' and l'_R are the usual left-handed lepton doublet and right-handed charged leptons respectively, Y_l and Y_Σ are the 3×3 Yukawa coupling matrices, and $\tilde{\Phi}_2 = i\sigma_2 \Phi_2^*$. Once the Higgs doublets Φ_1 and Φ_2 take Vacuum Expectation Value (VEV)

$$\langle \Phi_1 \rangle = \begin{pmatrix} 0 \\ v \end{pmatrix}, \quad \langle \Phi_2 \rangle = \begin{pmatrix} 0 \\ v' \end{pmatrix}, \tag{10}$$

we generate the following neutrino mass matrix

$$\mathcal{L}_\nu = \frac{1}{2} \begin{pmatrix} \overline{{\nu'}^C_{L_i}} & \overline{{\Sigma'}^0_{R_i}} \end{pmatrix} \begin{pmatrix} 0 & \frac{v'}{\sqrt{2}} Y^T_{\Sigma_{ij}} \\ \frac{v'}{\sqrt{2}} Y_{\Sigma_{ij}} & M_{ij} \end{pmatrix} \begin{pmatrix} {\nu'}_{L_j} \\ {\Sigma'}^{0\,C}_{R_j} \end{pmatrix} + h.c., \tag{11}$$

and the following charged lepton mass matrix

$$\begin{aligned} \mathcal{L}_l &= \begin{pmatrix} \overline{l'_{R_i}} & \overline{{\Sigma'}^-_{R_i}} \end{pmatrix} \begin{pmatrix} v Y_{l_{ij}} & 0 \\ v' Y_{\Sigma_{ij}} & M_{ij} \end{pmatrix} \begin{pmatrix} l'_{L_j} \\ {\Sigma'}^{+C}_{R_j} \end{pmatrix} + h.c., & (12) \\ &= \begin{pmatrix} \overline{l'_{R_i}} & \overline{{\Sigma'}^-_{R_i}} \end{pmatrix} M_l \begin{pmatrix} l'_{L_j} \\ {\Sigma'}^{+C}_{R_j} \end{pmatrix} + h.c., & (13) \end{aligned}$$

Note that due to the imposed Z_2 symmetry neutrino masses depend *only* on the new Higgs VEV v' while in the charged lepton mass matrix both the VEV's enter. The value of v' is determined by the scale of the neutrino masses and is independent of the mass scale of all other fermions. Therefore, the neutrino masses can be naturally light, without having to fine tune the Yukawas Y_Σ to unnaturally small values.

The 6×6 neutrino matrix (11) can be diagonalized to yield 3 light and 3 heavy Majorana neutrinos. The 6×6 unitary matrix U which accomplishes this is defined as

$$U^T \begin{pmatrix} 0 & m_D^T \\ m_D & M \end{pmatrix} U = \begin{pmatrix} D_m & 0 \\ 0 & D_M \end{pmatrix}, \quad \text{and} \quad \begin{pmatrix} {\nu'}_{L_j} \\ {\Sigma'}^{0\,C}_{R_j} \end{pmatrix} = U \begin{pmatrix} {\nu}_{L_j} \\ {\Sigma}^{0\,C}_{R_j} \end{pmatrix}, \tag{14}$$

[3]We will break this Z_2 symmetry mildly in the scalar potential. We discuss the phenomenological consequences of this Z_2 symmetry and its breaking when we introduce the scalar potential and present the Higgs mass spectrum in Appendix A.

where $m_D = v' Y_\Sigma/\sqrt{2}$, and

$$D_m = \begin{pmatrix} m_1 & 0 & 0 \\ 0 & m_2 & 0 \\ 0 & 0 & m_3 \end{pmatrix}, \quad D_M = \begin{pmatrix} M_{\Sigma_1} & 0 & 0 \\ 0 & M_{\Sigma_2} & 0 \\ 0 & 0 & M_{\Sigma_3} \end{pmatrix}. \tag{15}$$

Here m_i and M_{Σ_i} $(i = 1, 2, 3)$ are the low and high energy mass eigenvalues of the Majorana neutrinos respectively. We reiterate that the primed and unprimed notations represent the weak and mass eigenbases respectively. The mixing matrix U can be parameterized as a product of two matrices

$$U = W_\nu \, U_\nu \tag{16}$$

where W_ν is the matrix which brings the 6×6 neutrino matrix given by Eq. (11) in its block diagonal form as

$$W_\nu^T \begin{pmatrix} 0 & m_D^T \\ m_D & M \end{pmatrix} W_\nu \;=\; \begin{pmatrix} \tilde{m} & 0 \\ 0 & \tilde{M} \end{pmatrix}, \tag{17}$$

while U_ν diagonalizes $\tilde{m}_\nu$ and $\tilde{M}_\Sigma$ as

$$U_\nu^T \begin{pmatrix} \tilde{m} & 0 \\ 0 & \tilde{M} \end{pmatrix} U_\nu \;=\; \begin{pmatrix} D_m & 0 \\ 0 & D_M \end{pmatrix}. \tag{18}$$

The above parameterization therefore enables us to analytically estimate the mass eigenvalues and the mixing matrix U in terms of W_ν and U_ν by a two step process, by first calculating W_ν and then U_ν. Since the unitary matrix U has $6^2 = 36$ free parameters and the matrix U_ν has $2 \times 3^2 = 18$ parameter, the matrix W_ν should have $36 - 18 = 18$ free parameters. This matrix therefore can be parameterized as [29]

$$W_\nu = \begin{pmatrix} \sqrt{1 - BB^\dagger} & B \\ -B^\dagger & \sqrt{1 - B^\dagger B} \end{pmatrix}, \tag{19}$$

where $B = B_1 + B_2 + B_3 + ...$ and $B_j \sim (1/m_\Sigma)^j$, where m_Σ is the scale of the heavy Majorana fermion mass. Using an expansion in $1/m_\Sigma$ and keeping only terms second order or lower in $1/m_\Sigma$, we get

$$W_\nu \simeq \begin{pmatrix} 1 - \frac{1}{2} m_D^\dagger (M^{-1})^* M^{-1} m_D & m_D^\dagger (M^{-1})^* \\ -M^{-1} m_D & 1 - \frac{1}{2} M^{-1} m_D m_D^\dagger (M^{-1})^* \end{pmatrix}. \tag{20}$$

The light and heavy neutrino mass matrices obtained at this block diagonal stage are given by (only second order terms in $1/m_\Sigma$ are kept)

$$\tilde{m}_\nu \;=\; -m_D^T M^{-1} m_D, \tag{21}$$

$$\tilde{M} \;=\; M + \frac{1}{2} \left(m_D m_D^\dagger (M^{-1})^* + (M^{-1})^* m_D^* m_D^T \right). \tag{22}$$

Note that Eq. (21) is the standard seesaw formula for the light neutrino mass matrix, while Eq. (22) gives the heavy neutrino mass matrix. These can be diagonalized by two 3×3 unitary matrices U_0 and U_Σ, respectively. This yields

$$U_\nu = \begin{pmatrix} U_0 & 0 \\ 0 & U_\Sigma \end{pmatrix}, \tag{23}$$

For the charged leptons we follow an identical method for determining the mass eigenvalues and the mixing matrices. However, since the charged lepton mass matrix M_l given by Eq. (13) is a Dirac mass matrix, one has to diagonalize it using a bi-unitary transformation

$$T^\dagger \begin{pmatrix} m_l & 0 \\ \sqrt{2} m_D & M \end{pmatrix} S = \begin{pmatrix} D_l & 0 \\ 0 & D_H \end{pmatrix} = M_{l_d}, \tag{24}$$

where $m_l = v Y_l$, while D_l and D_H are diagonal matrices containing the light and heavy charged lepton mass eigenvalues. With the above definition for the diagonalization, the right-handed and left-handed weak and mass eigenbases for the charged leptons are related respectively as,

$$\begin{pmatrix} l'_L \\ \Sigma'^{+C}_R \end{pmatrix} = S \begin{pmatrix} l_L \\ \Sigma^{+C}_R \end{pmatrix}, \quad \text{and} \quad \begin{pmatrix} l'_R \\ \Sigma'^{+C}_R \end{pmatrix} = T \begin{pmatrix} l_R \\ \Sigma^{+}_R \end{pmatrix}. \tag{25}$$

Instead of using Eq. (24) for the diagonalization, we will work with the matrices

$$M_l^\dagger M_l = S\, M_{l_d}^\dagger M_{l_d}\, S^\dagger, \quad \text{and} \quad M_l M_l^\dagger = T\, M_{l_d} M_{l_d}^\dagger\, T^\dagger, \tag{26}$$

to obtain S and T respectively. As for the neutrinos, we parameterize

$$S = W_L U_L, \quad \text{and} \quad T = W_R U_R, \tag{27}$$

where W_L and W_R are the unitary matrices which bring $M_l^\dagger M_l$ and $M_l M_l^\dagger$ to their block diagonal forms, respectively,

$$W_L^\dagger\, M_l^\dagger M_l\, W_L = \begin{pmatrix} \tilde{m_l}^\dagger \tilde{m_l} & 0 \\ 0 & \tilde{M_H}^\dagger \tilde{M_H} \end{pmatrix}, \quad \text{and} \quad W_R^\dagger\, M_l M_l^\dagger\, W_R = \begin{pmatrix} \tilde{m_l} \tilde{m_l}^\dagger & 0 \\ 0 & \tilde{M_H} \tilde{M_H}^\dagger \end{pmatrix}. \tag{28}$$

Using arguments similar to that used for the neutrino sector, and keeping terms up to second order in $1/m_\Sigma$, we obtain

$$W_L \;=\; \begin{pmatrix} 1 - m_D^\dagger (M^{-1})^* M^{-1} m_D & \sqrt{2} m_D^\dagger (M^{-1})^* \\ -\sqrt{2} M^{-1} m_D & 1 - M^{-1} m_D m_D^\dagger (M^{-1})^* \end{pmatrix}, \tag{29}$$

$$W_R \;=\; \begin{pmatrix} 1 & \sqrt{2} m_l m_D^\dagger (M^{-1})^* M^{-1} \\ -\sqrt{2} (M^{-1})^* M^{-1} m_D m_l^\dagger & 1 \end{pmatrix}, \tag{30}$$

The square of the mass matrices for the light and heavy charged leptons in the flavor basis obtained after block diagonalization by W_R and W_L are given by

$$\begin{aligned} \tilde{m}_l \tilde{m}_l^\dagger &= m_l m_l^\dagger - 2 m_l m_D^\dagger (M^{-1})^* M^{-1} m_D m_l^\dagger, \quad (31) \\ \tilde{M}_H \tilde{M}_H^\dagger &= M M^\dagger + 2 m_D m_D^\dagger + (M^{-1})^* M^{-1} m_D m_l^\dagger m_l m_D^\dagger \\ &+ m_D m_l^\dagger m_l m_D^\dagger (M^{-1})^* M^{-1}, \quad (32) \end{aligned}$$

and

$$\begin{aligned} \tilde{m}_l^\dagger \tilde{m}_l &= m_l^\dagger m_l - [m_D^\dagger M^{*-1} M^{-1} m_D m_l^\dagger m_l + \text{h.c}] \quad (33) \\ \tilde{M}_H^\dagger \tilde{M}_H &= M^\dagger M + M^{-1} m_D m_D^\dagger M + M^\dagger m_D m_D^\dagger (M^{-1})^* + M^{-1} (m_D m_D^\dagger)^2 (M^{-1})^* \\ &+ [M^{-1} (M^{-1})^* M^{-1} m_D (m_l^\dagger m_l) m_D^\dagger M - \frac{1}{2} M^{-1} m_D m_D^\dagger M^{*-1} M^{-1} m_D m_D^\dagger M + \text{h.c}] \quad (34) \end{aligned}$$

One can explicitly check that the masses of the heavy charged leptons obtained from Eqs. (32) and (34) are approximately the same as that obtained for the neutral heavy fermion using Eq. (22). Indeed a comparison of these equations show that at tree level, the difference between the neutral and charged heavy fermions are of the order of the neutrino mass and can be hence neglected. One-loop effects bring a small splitting between the masses of the heavy and neutral fermions of ≈ 166 MeV. This allows the decay channel $\Sigma^\pm = \Sigma^0 + \pi^\pm$ at colliders, as discussed in detail in [18, 19]. In this paper we will neglect this tiny difference and assume that the masses of all heavy fermions are the same.

The matrices $\tilde{m}_l^\dagger \tilde{m}_l$ and $\tilde{M}_H^\dagger \tilde{M}_H$ are diagonalized by U_l and U_h^L giving,

$$U_L = \begin{pmatrix} U_l & 0 \\ 0 & U_h^L \end{pmatrix}. \quad (35)$$

Similarly the $\tilde{m}_l \tilde{m}_l^\dagger$ and $\tilde{M}_H \tilde{M}_H^\dagger$ matrices are diagonalized by U_r and U_h^R and hence give,

$$U_R = \begin{pmatrix} U_r & 0 \\ 0 & U_h^R \end{pmatrix}. \quad (36)$$

Finally, the low energy observed neutrino mass matrix is given by

$$U_{PMNS} = U_l^\dagger U_0. \quad (37)$$

Note that both U_l and U_0 are unitary matrices and hence U_{PMNS} is unitary.

3 A μ-τ Symmetric Model

As discussed in the introduction we wish to impose μ-τ symmetry on our model in order to comply with the current neutrino data, which shows a preference for $\theta_{13} = 0$ and $\theta_{23} = \pi/4$. Henceforth, we impose the μ-τ exchange symmetry on both the neutrino Yukawa matrix

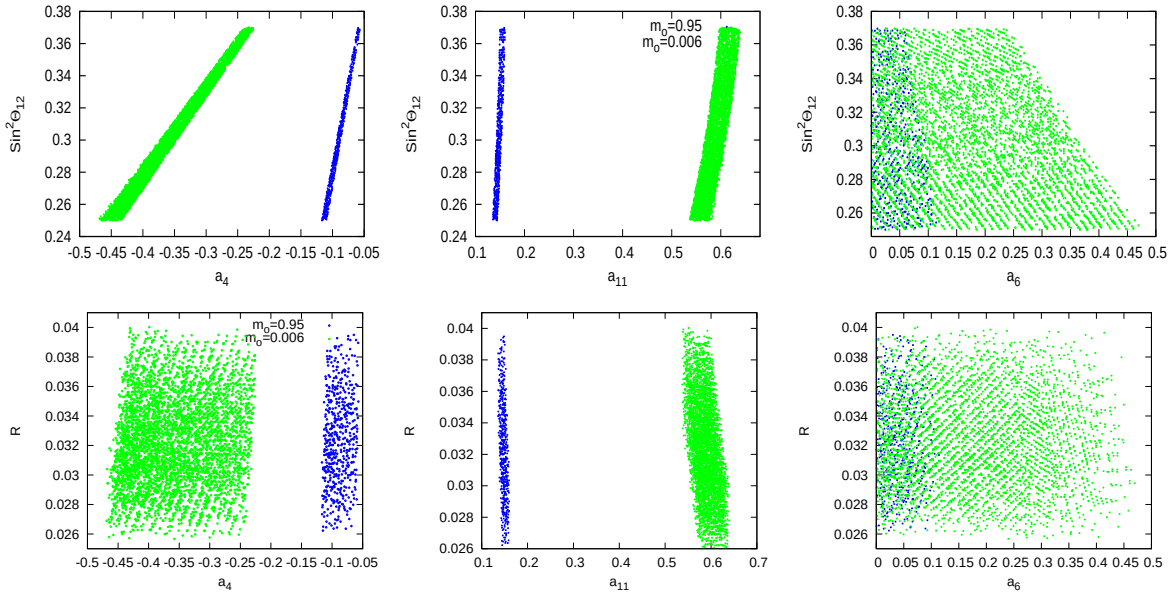

Figure 1: Scatter plots showing variation of $\sin^2\theta_{12}$ (upper panels) and $R = \Delta m^2_{21}/|\Delta m^2_{31}|$ (lower panels) as a function of a_4, a_{11} and a_6. All Yukawa couplings apart from the one plotted on the x-axis, are allowed to vary freely. Only points which predict oscillation parameters within their current 3σ values are shown. Blue points are for $m_0 = v'^2/(2M_1) = 0.95$ eV while the green points are for $m_0 = 0.006$ eV.

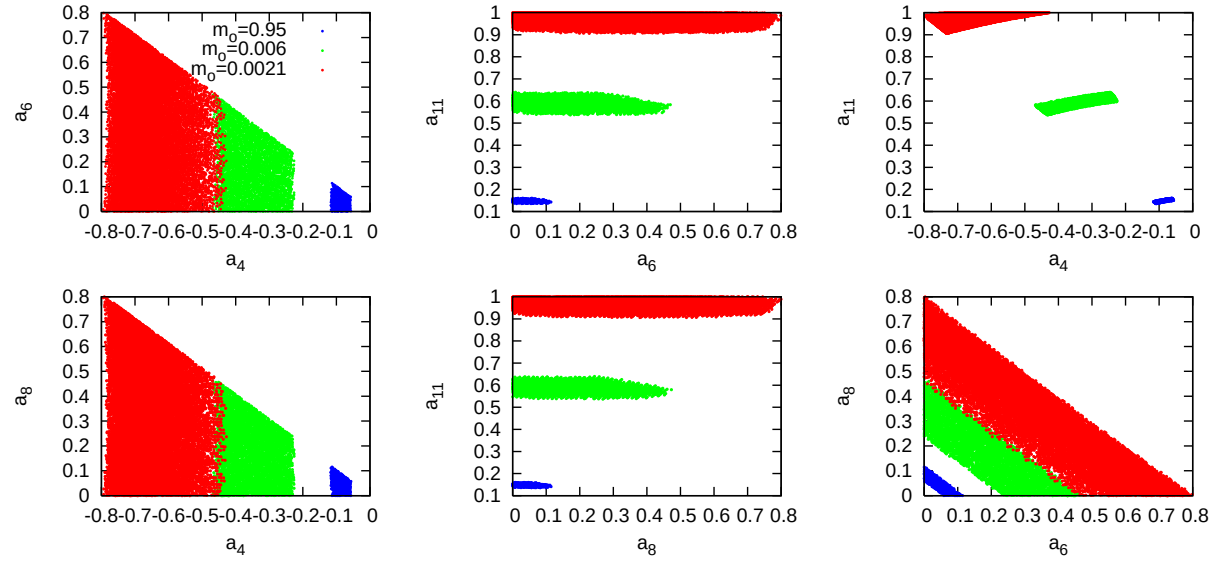

Figure 2: Scatter plot showing the values of the Yukawa couplings which give all oscillation parameters within their current 3σ allowed ranges. Allowed points are shown for $m_0 = 0.96$ eV (blue), 0.006 eV (green) and 0.0021 eV (red). All Yukawa couplings apart from the ones plotted in the x-axis and y-axis are allowed to vary freely, in each panel.

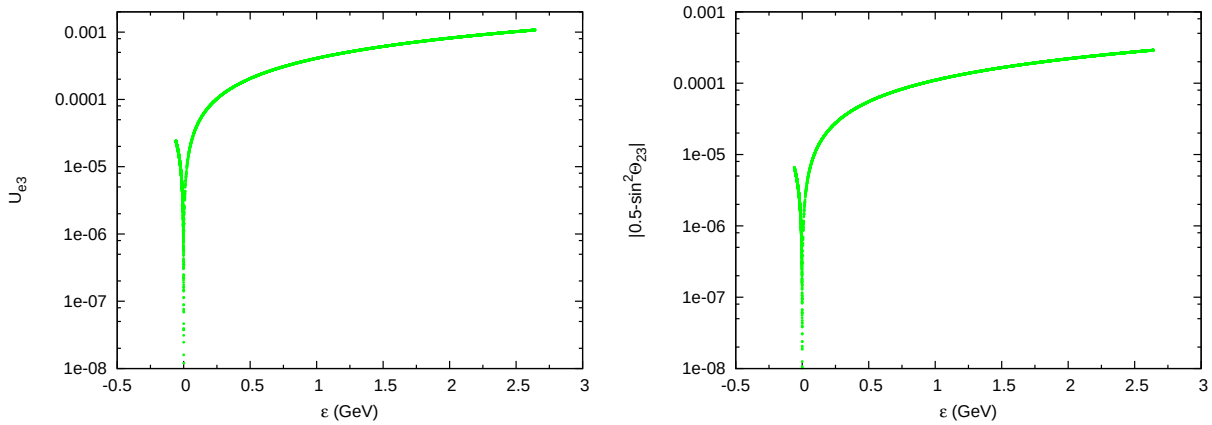

Figure 3: Non-zero values of U_{e3} and $|0.5 - \sin^2\theta_{23}|$ predicted when μ-τ symmetry is broken. Shown are the oscillation parameters against the μ-τ symmetry breaking parameter $\epsilon = M_3 - M_2$. Only points which reproduce the current neutrino observations within their 3σ C.L. are shown. The plot is generated at a fixed set of Yukawa couplings and heavy neutrino masses.

Y_Σ and the Majorana mass matrix for the heavy fermions M. Therefore, the neutrino Yukawa matrix takes the form

$$Y_\Sigma \;=\; \begin{pmatrix} a_4 & a_{11} & a_{11} \\ a'_{11} & a_6 & a_8 \\ a'_{11} & a_8 & a_6 \end{pmatrix}, \tag{38}$$

In what follows we will assume (for simplicity) that $a'_{11} = a_{11}$. Note that the μ-τ symmetry does not impose this condition. It only imposes that $Y_{\Sigma_{12}} = Y_{\Sigma_{13}}$ and $Y_{\Sigma_{21}} = Y_{\Sigma_{31}}$. We have put $a'_{11} = a_{11}$ in order to reduce the number of parameters in the theory. For the same reason, we assume all entries of Y_Σ to be real. The heavy Majorana mass matrix is given by

$$M \;=\; \begin{pmatrix} M_1 & 0 & 0 \\ 0 & M_2 & 0 \\ 0 & 0 & M_2 \end{pmatrix}, \tag{39}$$

where without loosing generality we have chosen to work in a basis where M is real and diagonal. Here the condition $M_3 = M_2$ is imposed due to the $\mu - \tau$ symmetry.

The above choice of Yukawa and heavy fermion mass matrix lead to the following form of the light neutrino mass matrix

$$\tilde{m} \simeq \frac{v'^2}{2} \begin{pmatrix} \frac{a_4^2}{M_1} + \frac{2a_{11}^2}{M_2} & a_{11}\left(\frac{a_4}{M_1} + \frac{a_6+a_8}{M_2}\right) & a_{11}\left(\frac{a_4}{M_1} + \frac{a_6+a_8}{M_2}\right) \\ a_{11}\left(\frac{a_4}{M_1} + \frac{a_6+a_8}{M_2}\right) & \frac{a_{11}^2}{M_1} + \frac{a_6^2+a_8^2}{M_2} & \frac{a_{11}^2}{M_1} + \frac{2a_6a_8}{M_2} \\ a_{11}\left(\frac{a_4}{M_1} + \frac{a_6+a_8}{M_2}\right) & \frac{a_{11}^2}{M_1} + \frac{2a_6a_8}{M_2} & \frac{a_{11}^2}{M_1} + \frac{a_6^2+a_8^2}{M_2} \end{pmatrix}, \tag{40}$$

where we have used the seesaw formula given by Eq. (21), which is valid up to second order in $1/m_\Sigma$. One can straightaway see from the above mass matrix that the scale of the neutrino masses emerges as $\sim v'^2 a^2/(2\, m_\Sigma)$, where a is a typical value of the Yukawa coupling in Eq. (38) and m_Σ the scale of heavy fermion masses. As discussed in the introduction, we restrict the heavy fermion masses to be less than 1 TeV in order that they can be produced at the LHC. Therefore in principle, neutrino masses of ~ 0.1 eV could have been obtained with just the standard model Higgs doublet by reducing the Yukawa couplings to values $\sim 10^{-6}$. However, this is usually considered as extreme fine tuning as there is no reason why the Yukawa couplings of the neutrinos should be so much suppressed, and the motivation for the seesaw mechanism is lost. In order to circumvent this, we introduced a different Higgs doublet Φ_2, which couples only to the exotic fermions. On the other hand, Yukawa coupling of the standard Higgs Φ_1 with the exotic fermions was forbidden in our model by the Z_2 symmetry. Hence, only the VEV of this new Higgs doublet appears in Eq. (40). Since this Higgs Φ_2 is not coupled to any standard model particle, it could have a VEV which could be different. Therefore, we demand that $v' \sim 10^5$ eV in order to generate neutrino masses of ~ 0.1 eV keeping the Yukawa couplings ~ 1. We have checked that such low value of Higgs VEV is not in conflict with any experimental data. We will discuss in detail the scalar potential and the Higgs mass spectrum in Appendix A.

We next turn to predictions of this model for the mass squared differences and the mixing angles. Since the neutrino mass matrix we obtained in Eq. (40) has μ-τ symmetry it follows that

$$\theta_{13} = 0 \;\; \text{and} \;\; \theta_{23} = \pi/4. \tag{41}$$

To find the mixing angle θ_{12} and the mass squared differences Δm^2_{21} and Δm^2_{31} [4], one needs to diagonalize the mass matrix $\tilde{m}$ given in Eq. (40). In fact, the form of $\tilde{m}$ in Eq. (40) is the standard form of the neutrino mass matrix with μ-τ symmetry, and hence the expression of mixing angle θ_{12} as well Δm^2_{21} and Δm^2_{31} can be found in the literature (see for *e.g.* [30]). We show in Fig. 1 the variation of $\sin^2\theta_{12}$ (upper panels) and $R = \Delta m^2_{21}/|\Delta m^2_{31}|$ (lower panels) with the Yukawa couplings a_4, a_{11} and a_6. We do not show the corresponding dependence on a_8 since it looks almost identical to the panel corresponding to a_6. The figure is produced assuming inverted mass hierarchy for the neutrino, *i.e.*, $\Delta m^2_{31} < 0$. The neutrino mass matrix given by Eq. (40) could very easily yield $\Delta m^2_{31} > 0$ and hence the normal mass hierarchy (see for *e.g.* [30]). However, for the sake of illustration, we will show results for only the inverted hierarchy in this paper. In every panel of Fig. 1, all Yukawa couplings apart from the one plotted on the x-axis, are allowed to vary freely. The points show the predicted values of $\sin^2\theta_{12}$ (upper panels) and R (lower panels) as a function of the Yukawa couplings for which all oscillation parameters are within their current 3σ values [31],

$$7.1 \times 10^{-5} eV^2 < \Delta m^2_{21} < 8.3 \times 10^{-5} eV^2 \;, \;\; 2.0 \times 10^{-3} eV^2 < |\Delta m^2_{31}| < 2.8 \times 10^{-3} eV^2 \;, \tag{42}$$

$$0.26 < \sin^2\theta_{12} < 0.42 \;, \quad \sin^2 2\theta_{23} > 0.9 \;, \quad \sin^2\theta_{13} < 0.05 \;. \tag{43}$$

[4] We define $\Delta m^2_{ij} = m^2_i - m^2_j$.

For this figure we take $M_1 = M_2$ for simplicity and define $m_0 = v'^2/(2M_1)$. The blue points are for $m = 0.95$ eV while the green points are for $m_0 = 0.006$ eV.

Fig. 2 is a scatter plot showing the values of the Yukawa couplings which give all oscillation parameters within their current 3σ allowed ranges given in Eqs. (42) and (43). Again as in the previous plot we assume $M_1 = M_2$, define $m_0 = v'^2/(2\,M_1)$ and show the allowed points for $m_0 = 0.96$ eV (blue), 0.006 eV (green) and 0.0021 eV (red). All Yukawa couplings apart from the ones shown in the x-axis and y-axis are allowed to vary freely, in each panel.

Since the μ and τ charged lepton masses are different, we phenomenologically choose to not impose the μ-τ symmetry on the charged lepton mass matrix[5]. Hence, without loosing generality, the charged lepton Yukawa matrix can be taken as

$$Y_l = \begin{pmatrix} Y_e & 0 & 0 \\ 0 & Y_\mu & 0 \\ 0 & 0 & Y_\tau \end{pmatrix}, \ . \tag{44}$$

The masses of the light charged leptons can then be obtained from Eqs. (31) and/or (33). For our choice of Y_Σ and M, it turns out that $m_e \approx vY_e$, $m_\mu \approx vY_\mu$, and $m_\tau \approx vY_\tau$, if we neglect terms proportional to v'^2. The mixing matrices U_l and U_r which diagonalize $\tilde{m}_l^\dagger \tilde{m}_l$ (cf. Eq. (33)) and $\tilde{m}_l \tilde{m}_l^\dagger$ (cf. Eq. (31)) respectively, turn out to be unit matrices at leading order.

$$U_l \simeq \begin{pmatrix} 1 & 0 & 0 \\ 0 & 1 & 0 \\ 0 & 0 & 1 \end{pmatrix}, \quad U_r \simeq \begin{pmatrix} 1 & 0 & 0 \\ 0 & 1 & 0 \\ 0 & 0 & 1 \end{pmatrix}, \tag{45}$$

Finally, we show in Fig. 3 the impact of μ-τ symmetry breaking on the low energy neutrino parameters. For the sake of illustration we choose a particular form for this breaking, by taking $M_3 \neq M_2$. Departure from μ-τ symmetry results in departure of U_{e3} from zero and $\sin^2\theta_{23}$ from 0.5. We show in Fig. 3 the U_{e3} (left hand panel) and $|0.5 - \sin^2\theta_{23}|$ generated as a function of the symmetry breaking parameter $\epsilon = M_3 - M_2$. The figure is generated for $a_4 = -0.066$, $a_{11} = 0.171$, $a_6 = 0.064$, $a_8 = 0.0037$ and $m_0 = 0.745$ eV. We have fixed $M_1 = M_2 = 299$ GeV in this plot. For $\epsilon = 0$, μ-τ symmetry is restored and both U_{e3} and $0.5 - \sin^2\theta_{23}$ go to zero. We show only points in this figure for which the current data can be explained within 3σ. We note that for $\epsilon > 0$ the curve extends to about $M_3 = M_2 + 2.6$ GeV, for this set of model parameters. For $\epsilon < 0$, the allowed range for ϵ is far more restricted.

We next turn our attention to the predictions of this model for the heavy fermion sector. The masses of the heavy fermions can be obtained using Y_Σ and M, as discussed in the previous section. The 6×6 mixing matrices, which govern the mixing of the heavy leptons with light ones, can also be obtained as discussed before. We will see in the next section that all the four 3×3 blocks of the matrices U, S and T are extremely important

[5]We reiterate that our choice of the lepton masses and mixing are dictated solely by observations.

for phenomenology at the LHC. We denote these 3×3 blocks as

$$U = \begin{pmatrix} U_{11} & U_{12} \\ U_{21} & U_{22} \end{pmatrix} = \begin{pmatrix} (W_\nu)_{11} U_0 & (W_\nu)_{12} U_\Sigma \\ (W_\nu)_{21} U_0 & (W_\nu)_{22} U_\Sigma \end{pmatrix}, \tag{46}$$

$$S = \begin{pmatrix} S_{11} & S_{12} \\ S_{21} & S_{22} \end{pmatrix} = \begin{pmatrix} (W_L)_{11} U_l & (W_L)_{12} U_h^L \\ (W_L)_{21} U_l & (W_L)_{22} U_h^L \end{pmatrix}, \tag{47}$$

$$T = \begin{pmatrix} T_{11} & T_{12} \\ T_{21} & T_{22} \end{pmatrix} = \begin{pmatrix} (W_R)_{11} U_r & (W_R)_{12} U_h^R \\ (W_R)_{21} U_r & (W_R)_{22} U_h^R \end{pmatrix}, \tag{48}$$

The matrices W_ν, W_L and W_R have been given in Eqs. (20), (29) and (30) respectively. These can be estimated for our choice of m_D, M and m_l. In particular, we note that S_{11} and T_{11} are close to 1, while U_{11} is given almost by U_{PMNS}. The off-diagonal blocks U_{12}, U_{21}, S_{12} and S_{21}, are suppressed by $\sim m_D/M$, while T_{12} and T_{21} are suppressed by $\sim m_D m_l/M^2$. Finally, the matrices $U_{22} = (W_\nu)_{22} U_\Sigma$, $S_{22} = (W_L)_{22} U_h^L$, and while $T_{22} \simeq U_h^R$. To estimate these we need to evaluate first the matrices which diagonalize the heavy fermion mass matrices $\tilde{M}$, $\tilde{M}_H^\dagger \tilde{M}_H$, and $\tilde{M}_H \tilde{M}_H^\dagger$ respectively. For M with μ-τ symmetry, it turns out that

$$U_\Sigma \simeq U_h^L \simeq U_h^R \simeq \begin{pmatrix} 1 & 0 & 0 \\ 0 & \frac{1}{\sqrt{2}} & -\frac{1}{\sqrt{2}} \\ 0 & \frac{1}{\sqrt{2}} & \frac{1}{\sqrt{2}} \end{pmatrix}, \tag{49}$$

thereby yielding

$$U_{22} \simeq \begin{pmatrix} 1 & 0 & 0 \\ 0 & \frac{1}{\sqrt{2}} & -\frac{1}{\sqrt{2}} \\ 0 & \frac{1}{\sqrt{2}} & \frac{1}{\sqrt{2}} \end{pmatrix}. \tag{50}$$

$$S_{22} \simeq \begin{pmatrix} 1 & 0 & 0 \\ 0 & \frac{1}{\sqrt{2}} & -\frac{1}{\sqrt{2}} \\ 0 & \frac{1}{\sqrt{2}} & \frac{1}{\sqrt{2}} \end{pmatrix}. \tag{51}$$

$$T_{22} \simeq \begin{pmatrix} 1 & 0 & 0 \\ 0 & \frac{1}{\sqrt{2}} & -\frac{1}{\sqrt{2}} \\ 0 & \frac{1}{\sqrt{2}} & \frac{1}{\sqrt{2}} \end{pmatrix}. \tag{52}$$

This structure of U_Σ, U_h^L and U_h^R (and hence of U_{22}, S_{22} and T_{22}), is an immediate consequence of the μ-τ symmetry in M and m_D. This is an extremely new and crucial feature. To the best of our knowledge, this has not been pointed out in any of the previous Type III seesaw models studies. The main reason is that no study so-far has considered the

flavor aspect of Type III seesaw. As a result none of them considered imposing an underlying flavor symmetry group on the fermions such that the triplet fermion Majorana mass matrix and the Yukawa matrix would be μ-τ symmetric. They assume that U_Σ, U_h^L and U_h^R are almost unit matrices since M is real and diagonal. However, this is true only if $M_1 \ll M_2 \ll M_3$. Breaking of the μ-τ symmetry either in m_D or in M, will destroy this non-trivial form for U_Σ, U_h^R and U_h^L. But having μ-τ symmetry in *both* Y_Σ and M is both theoretically as well as phenomenologically well motivated. We will see later that this non-trivial form of the matrices U_Σ, U_h^L and U_h^R will lead to certain distinctive signatures at LHC.

One should note that while U_Σ, U_h^L and U_h^R have the form given by Eq. (49), U_l and $U_r \simeq I$, though both M and Y_l were taken as real and diagonal. The main reason for this drastic difference is the following. While we take exact μ-τ symmetry for M, for Y_l we take a large difference between Y_μ and Y_τ values. This choice was dictated by the observed charged lepton masses.

Finally, a comment regarding the extent of deviation from unitarity in our model is in order. It is clear from the discussion of the previous section and Eq. (20) that the deviation from unitarity of the light neutrino mixing matrix is $\propto m_D^2/m_\Sigma^2 \simeq m_\nu/m_\Sigma$, where m_ν and m_Σ are the light neutrino and heavy lepton mass scales respectively. Therefore, an important difference between our model and the usual GUT Type III seesaw models is that the extent of non-unitarity for our model is much larger. This will result in larger lepton flavor violating decays in our case. Detailed calculations for lepton flavor violating radiative as well as tree level decays of a generic Type III seesaw model have been published in [14, 15] and we do not repeat them here. The authors of these papers have also worked out the current constraints on the deviation from unitarity. One can check that even for 100-1000 GeV mass range heavy leptons, the predicted non-unitarity and lepton flavor violating decay rates in our model are far below the current experimental bounds. In fact, the predicted decay rates can be seen to be far below the sensitivity reach of all forthcoming experiments.

4 Heavy Fermion Production at LHC

The triplet fermions couple to the standard model particles through the Yukawa couplings as well as gauge couplings. We give in Appendix B, the detailed Yukawa and gauge couplings of the neutral and charged heavy fermions with the standard model leptons, vector bosons, and Higgs particles. We have kept the masses of the heavy fermions in the 100 GeV to 1 TeV range. Therefore, it should be possible to produce these fermions at LHC. In this section, we will study in depth the production and detection possibilities of the heavy leptons in our Type III seesaw model. Compared to the earlier papers, there are two distinctly new aspects in our analysis – (i) presence of two Higgs doublet instead of one, leading to a far more rich collider phenomenology, (ii) presence of μ-τ symmetry in our model.

The heavy triplet fermion production at LHC has been discussed by many earlier papers

[17–21]. At LHC we will be looking at the following production channels

$$pp \to \Sigma^{\pm}\Sigma^{\mp}, \Sigma^{\pm}\Sigma^{0}, \Sigma^{0}\Sigma^{0}.$$

The exotic fermions have both Yukawa couplings to Higgs as well as gauge couplings to vector bosons. Therefore, they could be in principle produced through either gauge mediated partonic processes (left diagram) or through Higgs mediated partonic processes (right diagram)

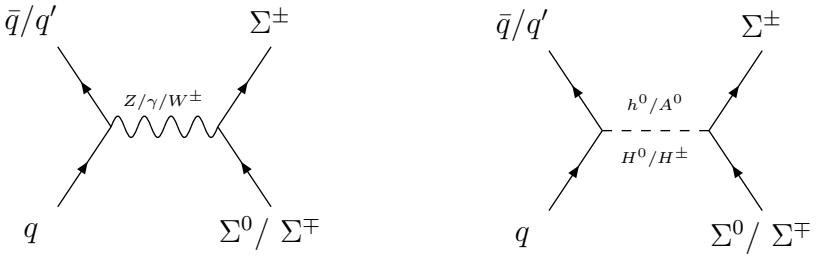

However, it turns out that the vertex factors for the couplings of heavy fermions to gauge bosons which are relevant for the formers production, *viz.*, $\Sigma^+\Sigma^- Z/\gamma$ and $\Sigma^0\Sigma^{\pm}W^{\mp}$, are much larger than those involving the Higgs, *viz.*, $\Sigma^+\Sigma^- H^0/h^0/A^0$ and $\Sigma^0\Sigma^{\pm}H^{\mp}$. To illustrate this with a specific example, we compare the $\Sigma^+\Sigma^- Z$ coupling given in Eqs. (B16) and (B17) with the $\Sigma^+\Sigma^- h^0$ coupling given in Table 9. It is easy to see that the $\Sigma^+\Sigma^- Z/\gamma$ coupling has terms proportional to $T_{22}^{\dagger}T_{22}$ and $S_{22}^{\dagger}S_{22}$, while the $\Sigma^+\Sigma^- h^0$ coupling depends on terms which have an off-diagonal mixing matrix block. Since the off-diagonal mixing matrix blocks are much smaller than the diagonal ones (as discussed in section 3), it is not surprising that the couplings of two exotic fermions to the Higgs particles are much smaller than to the gauge bosons. Hence the heavy exotic fermions will be produced predominantly via the gauge boson mediated processes. For the heavy fermion production cross-section at the LHC, we chose CTEQ6L [32] as the parton distribution function (PDF) and partonic center of mass energy as the renormalization and factorization scale. We have explicitly checked that the production cross-sections do not change much with the PDF and scale. All cross-sections in this paper are calculated using the Calchep package [33].

In Fig. 4 we show the production cross-section for $\Sigma^-\Sigma^0$ (bold dotted line), $\Sigma^+\Sigma^0$ (solid line), and $\Sigma^+\Sigma^-$ (fine dotted line), at LHC as a function of the corresponding heavy fermion mass. It is straightforward to see that the $\Sigma'^0\Sigma'^0 Z$ (and $\Sigma'^0\Sigma'^0 W^{\pm}$) couplings are absent. A very small $\Sigma^0\Sigma^0 Z$ is generated through mixing from the $\nu'^0\nu'^0 Z$ coupling. However, this is extremely small. Hence, $\Sigma^0\Sigma^0$ production through gauge interactions is heavily suppressed and is not shown in Fig. 4. One can see that the production cross-sections of the heavy fermions fall sharply with their mass. More precisely, $\sigma(\Sigma^{\pm}\Sigma^{\mp}) = 112$ fb, $\sigma(\Sigma^+\Sigma^0) = 206$ fb and $\sigma(\Sigma^-\Sigma^0) = 95$ fb, for $M_{\Sigma_i} \simeq 300$ GeV. However, for $M_{\Sigma_i} \simeq 600$ GeV this quickly falls to $\sigma(\Sigma^{\pm}\Sigma^{\mp}) = 6$ fb, $\sigma(\Sigma^+\Sigma^0) = 13$ fb, and $\sigma(\Sigma^-\Sigma^0) = 4$ fb. Therefore, it is obvious that the lightest amongst the three generation of heavy fermions will be predominantly produced at the collider, and will hence dominate the phenomenology. One can check that the production cross-sections that we get is almost identical to that obtained in earlier

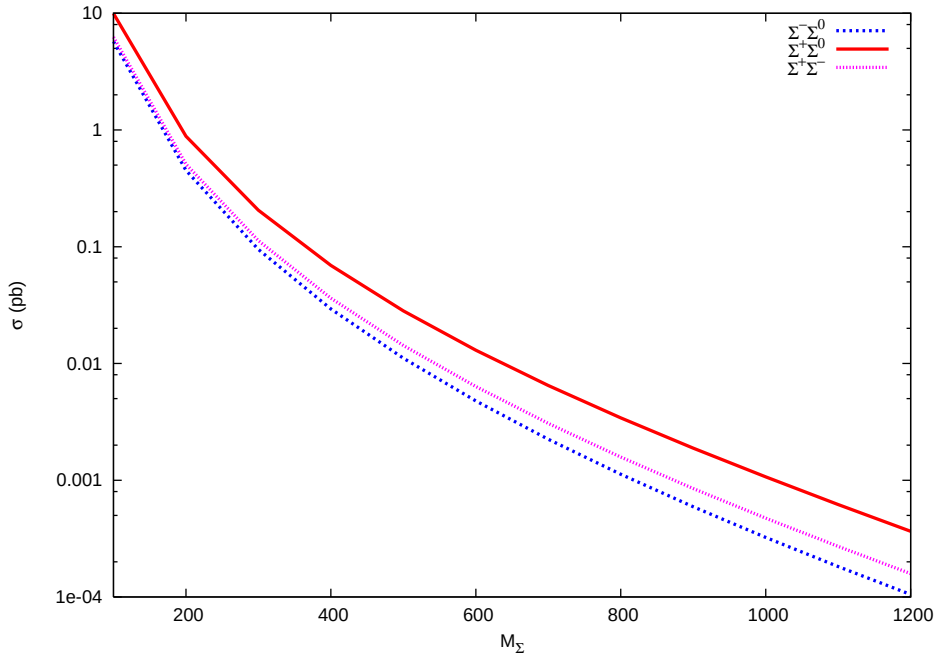

Figure 4: Variation of production cross section of $\Sigma^{\pm}$, Σ^0 with the mass of exotic leptons.

papers [19, 20]. This is not unexpected since our model is different from all the earlier models in the Higgs sector. However as discussed above, it is the gauge interactions which predominantly produce the exotic leptons. The gauge-lepton couplings in our model is same as in the earlier works. Since the heavy fermion production comes mostly from the gauge mediated sub-processes, we get the same production cross-sections as other papers.

5 Heavy Fermion Decays

Once produced at LHC, the heavy fermions will decay to different lighter states due to its interaction with different standard model particles. In particular, they could decay into light leptons and Higgs due to their Yukawa couplings, or to light leptons and vector bosons due to their gauge interactions. The light leptons could be either the charged leptons or the neutrinos. The Higgs could be either the neutral Higgs h^0, H^0, A^0, or the charged Higgs $H^{\pm}$. The gauge bosons could be either $W^{\pm}$ or Z. The Higgs and gauge bosons would eventually give the final state particles in the detector, which will be tagged at the experiment. This will be studied in detail in the following sections. Here we concentrate on only the two body decay rates and branching ratios of the exotic leptons $\Sigma^{\pm}$ and Σ^0. All possible vertices and the corresponding vertex factors for the Yukawa interactions of $\Sigma^{\pm}$ and Σ^0 are given in Tables 9, 10, 11. The vertices and vertex factors for the charged and neutral current gauge interactions can be found in Appendix B.2. Presence of two Higgs doublets and μ-τ symmetry in Y_{Σ} and M will have direct implications in the partial

decay widths for different decay processes.

5.1 Decay to Light Leptons and Higgs

In this subsection, we perform a detailed study of all two-body decays of these fermions into a lepton and a Higgs. Since we have two Higgs doublets in our model, we have a pair of charged Higgs $H^{\pm}$, and three neutral Higgs – h^0 and H^0 are CP even, while A^0 is CP odd. The Higgs mass spectrum and mixing is given in Appendix A. The decay width Γ for $\Sigma_i \to l_j X$ is given by

$$\Gamma = \frac{M_{\Sigma_i}}{32\pi}\Big[1 - \frac{(M_X - m_{l_j})^2}{{M_{\Sigma_i}}^2}\Big]^{\frac{1}{2}} \times \Big[1 - \frac{(M_X + m_{l_j})^2}{{M_{\Sigma_i}}^2}\Big]^{\frac{1}{2}} \times A_{ji}, \tag{53}$$

where M_{Σ_i}, M_X and m_{l_j} are the masses of $\Sigma_i^0/\Sigma_i^{\pm}$, X and l_j, respectively, where X is the relevant Higgs involved. The l_j could be either a charged lepton or a neutrino. For the charged Higgs $H^{\pm}$ mode, and the neutral Higgs h^0 and H^0 mode, the factor A_{ji} is given as

$$\begin{aligned} A_{ji} &= \Big(|(C_{l\Sigma}^{X,L})_{ji}|^2 + |(C_{l\Sigma}^{X,R})_{ji}|^2\Big)\Big(1 - \frac{(M_X^2 - M_l^2)}{M_{\Sigma_i}^2}\Big) \\ &\quad + \Big((C_{l\Sigma}^{X,L})^*_{ji}(C_{l\Sigma}^{X,R})_{ji} + (C_{l\Sigma}^{X,R})^*_{ji}(C_{l\Sigma}^{X,L})_{ji}\Big)\frac{m_{l_j}}{M_{\Sigma_i}}, \end{aligned} \tag{54}$$

while for the CP-odd neutral Higgs A^0 the factor is

$$\begin{aligned} A_{ji} &= \Big(|(C_{l\Sigma}^{X,L})_{ji}|^2 + |(C_{l\Sigma}^{X,R})_{ji}|^2\Big)\Big(1 - \frac{(M_X^2 - M_l^2)}{M_{\Sigma_i}^2}\Big) \\ &\quad - \Big((C_{l\Sigma}^{X,L})^*_{ji}(C_{l\Sigma}^{X,R})_{ji} + (C_{l\Sigma}^{X,R})^*_{ji}(C_{l\Sigma}^{X,L})_{ji}\Big)\frac{m_{l_j}}{M_{\Sigma_i}}. \end{aligned} \tag{55}$$

In the above equations $(C_{l\Sigma}^{X,L})/(C_{l\Sigma}^{X,R})$ are the relevant vertex factors given in Table 9, 10 and 11, and i, j represents the generation. In all numerical results that follow we will fix the model parameters (Yukawa couplings and entries of M mass matrix) to their values given in Table 1. This set of model parameters yield $\Delta m_{21}^2 = 7.67\times10^{-5}$ eV^2, $\Delta m_{31}^2 = -2.435\times10^{-3}$ eV^2 and $\sin^2\theta_{12} = 0.33$. Of course $\theta_{13} = 0$ and $\theta_{23} = \pi/4$. Throughout the rest of the paper, we also take the value of $M_{h^0} = 40$ GeV, $M_{H^0} = 150$ GeV, $M_{A^0} = 140$ GeV and $M_{H^{\pm}} = 170$ GeV. Also, for all cases where we present results for fixed values of the heavy fermion masses, we take $M_{\Sigma_1} = 300$ GeV and $M_{\Sigma_2} = M_{\Sigma_3} = 600$ GeV.

5.1.1 $\Sigma^{\pm} \to l^{\pm} h^0/H^0/A^0$

Let us begin with the decay of heavy charged leptons into light charged leptons and neutral Higgs. The Higgs concerned in this case could be h^0, H^0, or A^0. We start by probing the decay rate $\Sigma_i^{\pm} \to l_j^{\pm} h^0$. From Eq. (53) we see that the decay rate is governed by the factor A_{ji}, which in turn depends on the vertex factors given in Table 9. The vertex factors are

a_4	a_6	a_8	a_{11}	m_o/eV	$\frac{M_2}{M_1}$	$\frac{M_3}{M_1}$
0.145	0.097	0.109	4×10^{-4}	2.356	2.0	2.0

Table 1: Model parameters used for all numerical results in section 5 and 6. This set of model parameters yield $\Delta m^2_{21} = 7.67 \times 10^{-5}$ eV^2, $\Delta m^2_{31} = -2.435 \times 10^{-3}$ eV^2 and $\sin^2\theta_{12} = 0.33$. Of course $\theta_{13} = 0$ and $\theta_{23} = \pi/4$. Parameter $m_0 = v'^2/(2M_1)$.

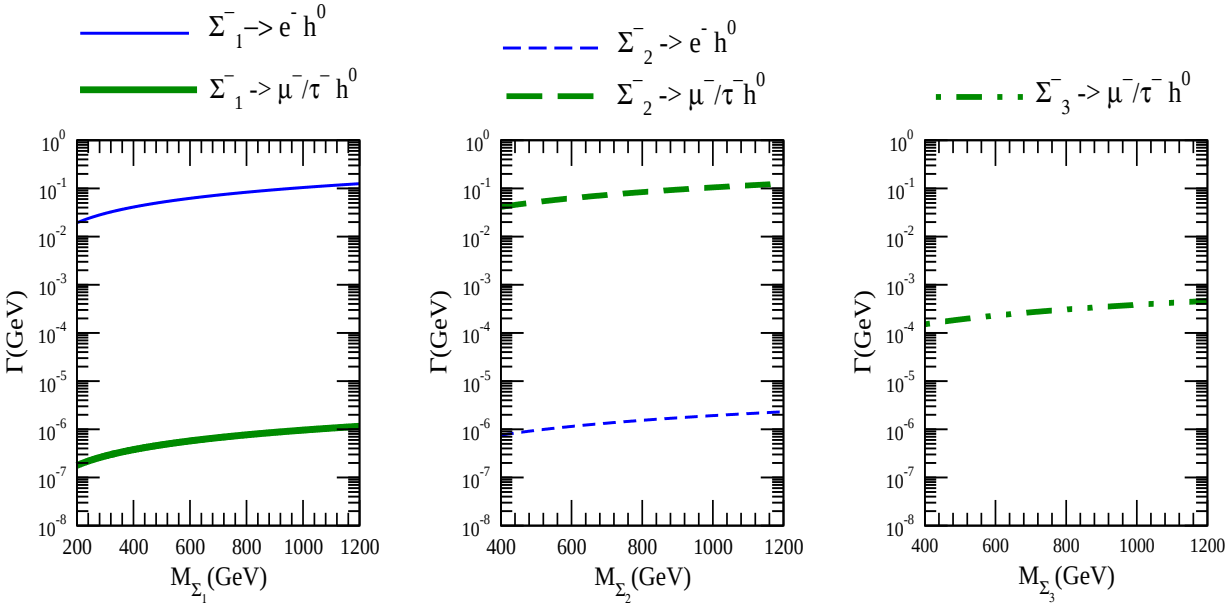

Figure 5: Variation of $\Gamma(\Sigma_i^- \to l_j^- h^0)$ with M_{Σ_i}

given in terms of the 3×3 block matrices S_{ab} and T_{ab}, where $a, b = 1, 2$. We have seen in the earlier sections that S_{12}, T_{12} and T_{21} are heavily suppressed – the first one by $\mathcal{O}(m_D/M)$ and T_{12} and T_{21} by $\mathcal{O}((m_l m_D)/M^2)$. The vertex factors also depend on the Higgs mixing angle α. In Appendix A, we have shown how the neutrino mass constrains the neutral Higgs mixing such that $\sin\alpha \sim 10^{-6}$ and $\cos\alpha \sim 1$. Therefore, for the $\Sigma_i^\pm \to l^\pm h^0$ decay the dominating vertex factor is

$$C^{h^0,R}_{l^\pm\Sigma^\pm} \simeq \frac{1}{\sqrt{2}} S_{11}^\dagger Y_\Sigma^\dagger T_{22} \cos\alpha. \tag{56}$$

We have seen in Eq. (47) that $S_{11} \simeq 1$ if we neglect terms of the order of $\mathcal{O}(m_D^2/M^2)$. Therefore,

$$C^{h^0,R}_{l^\pm\Sigma^\pm} \simeq \begin{pmatrix} a_4 & \sqrt{2}a_{11} & 0 \\ a_{11} & \frac{1}{\sqrt{2}}(a_6+a_8) & \frac{1}{\sqrt{2}}(a_8-a_6) \\ a_{11} & \frac{1}{\sqrt{2}}(a_6+a_8) & \frac{1}{\sqrt{2}}(a_6-a_8) \end{pmatrix}. \tag{57}$$

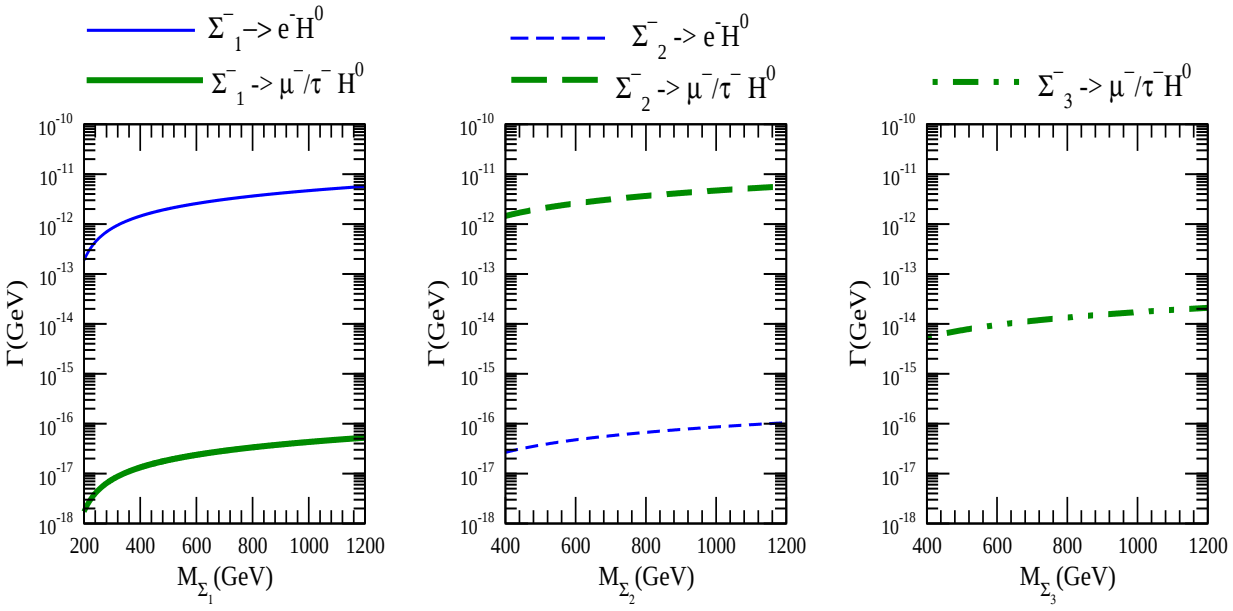

Figure 6: Variation of $\Gamma(\Sigma_i^- \to l_j H)$ with M_{Σ_i}

From Eq. (57) we can see that $(C^{h^0,R}_{l^\pm\Sigma^\pm})_{13} \simeq 0$. In fact one can check that this happens because T_{22} given by Eq. (52) has a specific form, which is due to μ-τ symmetry. The consequence of this is that decay of $\Sigma_3^- \to e^- h^0$ will be forbidden to leading order. Also note from Eq. (57) that the decay rate of all heavy charged fermions into $\mu^\pm$ is predicted to be exactly equal to their decay rate into $\tau^\pm$. This is also an obvious consequence of the μ-τ symmetry.

The partial decay widths for $\Sigma_i^- \to l_j^- h^0$ from an exact numerical calculation in shown in Fig. 5, as a function of the heavy charged fermion mass. The thin blue lines are decay into e^-, while the thick green lines are for decay into μ^-/τ^-. As expected, we notice the following two consequences of μ-τ symmetry

- Decay rate of $\Sigma_3^- \to e^- h^0$ is almost zero.
- The decay rate of the heavy fermions into μ^- is exactly equal to that into τ^-.

We can also see that for Σ_1^- decay, the decay rate into e^- is about 5 orders of magnitude larger than into μ^-/τ^-. The trend is opposite for Σ_2^- decay, where the decay is predominantly into μ^-/τ^-. Both of these features can be understood from Eq. (57) and the values of the Yukawa couplings taken (cf. Table 1). Σ_1^- decay into e^- and μ^-/τ^- is proportional to a_4^2 and a_{11}^2, respectively. The ratio of the decay widths seen in the figure matches the ratio $a_4^2/(a_{11}^2) \sim 10^5$. Similarly, one can check that for Σ_2^- decay, the corresponding ratio is $4a_{11}^2/(a_6 + a_8)^2$, which agrees with the middle panel of Fig. 5. Finally, the fact that the decay rate of $\Sigma_3^- \to \mu^- h^0$ is less than that of $\Sigma_2^- \to \mu^- h^0$ can also be understood in terms of Eq. (57) and the Yukawa coupling values taken for the calculation.

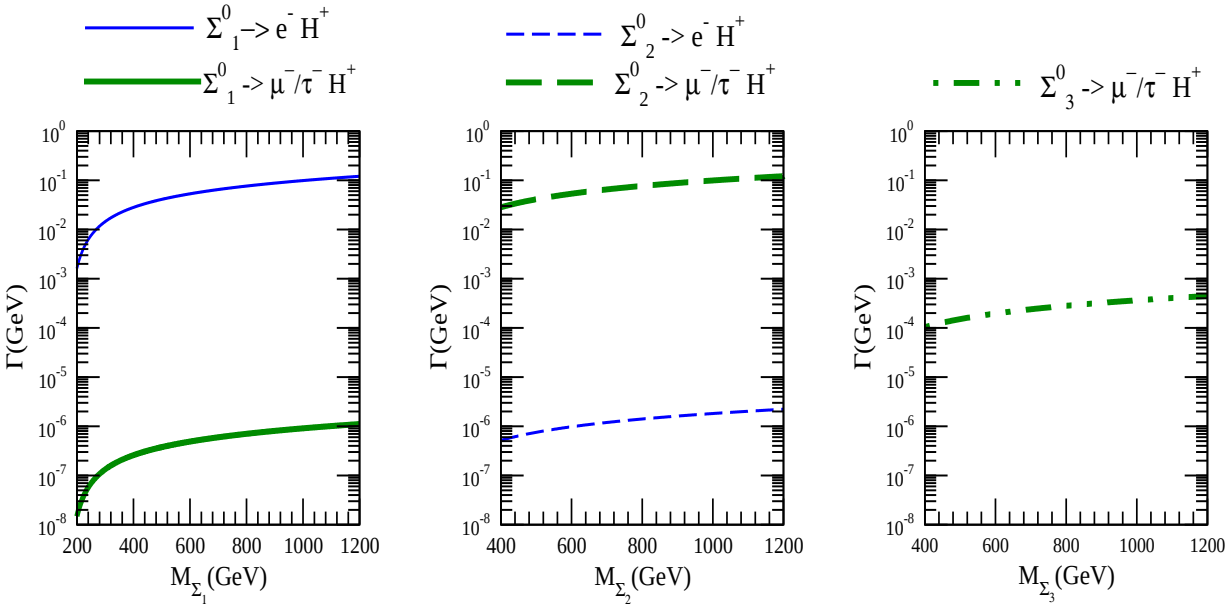

Figure 7: Variation of $\Gamma(\Sigma_i^0 \to l_j H^+)$ with M_{Σ_i}

We next turn to the decay width for $\Sigma_i^\pm \to l_j^\pm H^0$. Expression for the decay rate is same as that given by Eq. (53) except that now M_{h^0} is replaced by the H^0 mass M_{H^0}. For this decay channel the A_{ji} factor is dominantly given by

$$C_{l^\pm \Sigma^\pm}^{H^0,R} \simeq \frac{1}{\sqrt{2}} S_{11}^\dagger Y_\Sigma^\dagger T_{22} \sin\alpha. \tag{58}$$

Note that compared to the effective vertex factor for $\Sigma_i^\pm \to l_j^\pm h^0$ given in Eq. (56), the effective vertex factor given above for $\Sigma_i^\pm \to l_j^\pm H^0$ is suppressed by $\sin\alpha$. Since $\sin\alpha \sim 10^{-6}$, the decay rate of $\Sigma_i^\pm$ into H^0 are heavily suppressed. We show in Fig. 6 this decay rate calculated from exact numerical results. Comparing Fig. 5 with Fig. 6, we see that decays into H^0 are suppressed by a factor of about $\sim 10^{10}$, as expected from the order of magnitude estimate. Therefore, we can neglect $\Sigma_i^\pm \to l_j^\pm H^0$ for all practical purposes.

From Table 9 it is easy to see that the decay rate $\Sigma_i^\pm \to l_j^\pm A^0$ will be almost identical to that that predicted for $\Sigma_i^\pm \to l_j^\pm h^0$. The vertex factors for the two process are the same and hence the only difference could come from the difference between the Higgs masses. However, it is easy to see from Eq. (53) that the effect of the Higgs mass on the decay rate is not very significant, especially for relatively heavy fermions.

5.1.2 $\Sigma^0 \to l^\mp H^\pm$

The decay rate for this channel is also given by Eq. (53), and is governed primarily by the vertex factor

$$C^{H^\pm,R}_{l^\pm\Sigma^0} \simeq \frac{1}{\sqrt{2}} S^\dagger_{11} Y^\dagger_\Sigma U^*_{22} \cos\beta. \tag{59}$$

Recall that $\cos\beta \sim 1$. As discussed before, the matrix U_{22} displays features similar to the matrix T_{22}. Therefore, the form of dominant vertex factor for this case is similar to that given in Eq. (57). The corresponding decay rates are shown in Fig. 7. All features seen for $\Sigma_i^- \to l_j h^0$ is also seen here. Decay channel $\Sigma_3^0 \to e_j^\mp H^\pm$ is forbidden. Decay rates to $\mu^\mp$ is equal to decay rate to $\tau^\mp$. The huge hierarchy in the decay rates of Σ_1^0 and Σ_2^0 into e and μ/τ are also present due to same reason as given for $\Sigma^- \to l^- h^0$ decays. The decay rate and flavor structure for the final state charged leptons is therefore seen to be same here as for the decay of charged heavy fermions into charged light leptons and h^0. However, in this case we have a charged Higgs in the final state and it should be easy to tag this and differentiate the two processes in the detector at LHC. We will also discuss in the following sections that the h^0 also has a much longer lifetime than $H^\pm$, which can be observed in the detector. In addition, the heavy lepton itself is charged in one case and uncharged in the other. The two processes should hence be separable at the collider experiment.

5.1.3 $\Sigma^0 \to \nu\, h^0/H^0/A^0$

We next turn to the decay channels with a light neutrino in the final state. This will give missing energy in the final state. Decay of the neutral Σ^0 will create a neutrino and a neutral Higgs. As in the case of decay of $\Sigma^\pm$ to charged leptons and neutral Higgs, one can check from Table 10 that the decay to the Higgs H^0 is heavily suppressed due to smallness of U_{21} as well as the $\sin\alpha$ term. However, decay to h^0 is driven by the vertex factor

$$C^{h^0,R}_{\nu\Sigma^0} = \frac{1}{2} U^\dagger_{11} Y^\dagger_\Sigma U^*_{22} \cos\alpha. \tag{60}$$

For the decay $\Sigma_i^0 \to \nu_j A^0$ we find from Table 10 that the dominant vertex factor is

$$C^{A^0,R}_{\nu\Sigma^0} = -\frac{i}{2} U^\dagger_{11} Y^\dagger_\Sigma U^*_{22} \cos\beta. \tag{61}$$

Since $\cos\beta \simeq \cos\alpha$, the decay rate and flavor structure for this channel will be similar to what we found for the $\Sigma_i^0 \to \nu_j h^0$ channel. The main difference comes in the difference between the masses of the h^0 and A^0 Higgs.
For the $\Sigma_i^0 \to \nu_j H^0$ decay, one can see from Table 10 that the vertex factors for both P_L as well as P_R vertices, are suppressed by $\sin\alpha$. Therefore, this decay rate can be neglected.

5.1.4 $\Sigma^{\pm} \to \nu\, H^{\pm}$

From Table 11 the vertex factor for this decay will be

$$C_{\nu\Sigma^{\pm}}^{H^{\pm},L} \simeq U_{11}^T Y_\Sigma^T S_{22} \cos\beta. \tag{62}$$

As we have seen in section 3, the structure of S_{22} is very similar to that of U_{22}. Hence, a comparison of the vertex factor for this process with the one from $\Sigma_i^0 \to \nu_j h^0$ and $\Sigma_i^0 \to \nu_j A^0$ shows that all three will have decay rates of comparable magnitude, modulo the difference in the masses of the scalars h^0, A^0 and $H^{\pm}$. Since we assume masses of h^0, A^0 and $H^{\pm}$ as 40 GeV, 140 GeV and 170 GeV respective, the decay rate for $\Sigma^{\pm} \to \nu H^{\pm}$ is predicted to be the lowest.

5.2 Decay to Light Leptons and Vector Bosons

The exotic heavy leptons have gauge interactions. Therefore, it is expected that they will also decay into final state particles with vector bosons, $W^{\pm}$ and Z. The decay width Γ for $\Sigma_i^{\pm} \to l_j^{\pm}/\nu V$ and $\Sigma_i^0 \to l_j^{\pm}/\nu V$ in the $m_l = 0$ limit is given by

$$\Gamma = \frac{M_{\Sigma_i}}{32\pi}\Big[1 - \frac{{M_V}^2}{{M_\Sigma}^2}\Big]^2 \Big[2 + \frac{{M_\Sigma}^2}{{M_V}^2}\Big]\Big(|(C_{l^{\pm}\Sigma}^{V,L})_{ji}|^2 + |(C_{l^{\pm}\Sigma}^{V,R})_{ji}|^2\Big), \tag{63}$$

where $C_{l^{\pm}\Sigma}^{V,L}$ and $C_{l^{\pm}\Sigma}^{V,R}$ are the relevant vertex factors given in Appendix B.2, and M_V is the mass of the vector boson involved. The dominant vertex factor relevant for $\Sigma^{\pm} \to l^{\pm} Z$ and $\Sigma^0 \to l^{\pm} W^{\mp}$ in terms of Y_Σ, M, v' and the mixing matrices are given respectively by

$$C_{l^{\pm}\Sigma^{\pm}}^{Z,L} \simeq \frac{v'}{2}\,\frac{g}{c_w}\, U_l{}^{\dagger} Y_\Sigma^{\dagger} M^{-1} U_h^L, \quad \text{and} \quad C_{l^{\pm}\Sigma^0}^{W^{\mp},L} \simeq -\frac{v'}{2}\, g\, U_l{}^{\dagger} Y_\Sigma^{\dagger} M^{-1} U_\Sigma. \tag{64}$$

For the other two channels $\Sigma^0 \to \nu Z$ and $\Sigma^{\pm} \to \nu W^{\pm}$, they are given respectively by

$$C_{\nu\Sigma^0}^{Z,L} \simeq \frac{v'}{2\sqrt{2}}(g c_w + g' s_w) U_{PMNS}^{\dagger} Y_\Sigma^{\dagger} M^{-1} U_\Sigma, \quad \text{and} \quad C_{\nu\Sigma^{\pm}}^{W^{\mp},R} \simeq -\frac{v'}{\sqrt{2}}\, g\, U_{PMNS}^T Y_\Sigma^T M^{-1} U_h^R. \tag{65}$$

As mentioned before, the gauge interaction part of our model is identical to that for the one Higgs doublet Type III seesaw considered earlier. Some of these vertex factors[6] can therefore can be seen to agree with that given in [15]. The only difference is that we include the matrices U_l, U_h^R and U_Σ in our general expressions, while these were taken as unit matrices in [15].

5.3 Comparing $\Sigma^{\pm/0}$ Decays to Higgs and Gauge Bosons

In Fig. 8 we show the decay rates $\Sigma_1^- \to \nu_1 W^-$ (long-dashed blue line), $\Sigma_1^- \to e^- Z$ (dot-dashed green line), $\Sigma_1^0 \to \nu_1 Z$ (dot-dashed magenta line), $\Sigma_1^0 \to e^- W^+$ (thin solid red line),

[6] Vertex factor for $\Sigma^0 \to \nu Z$ is not given in [15].

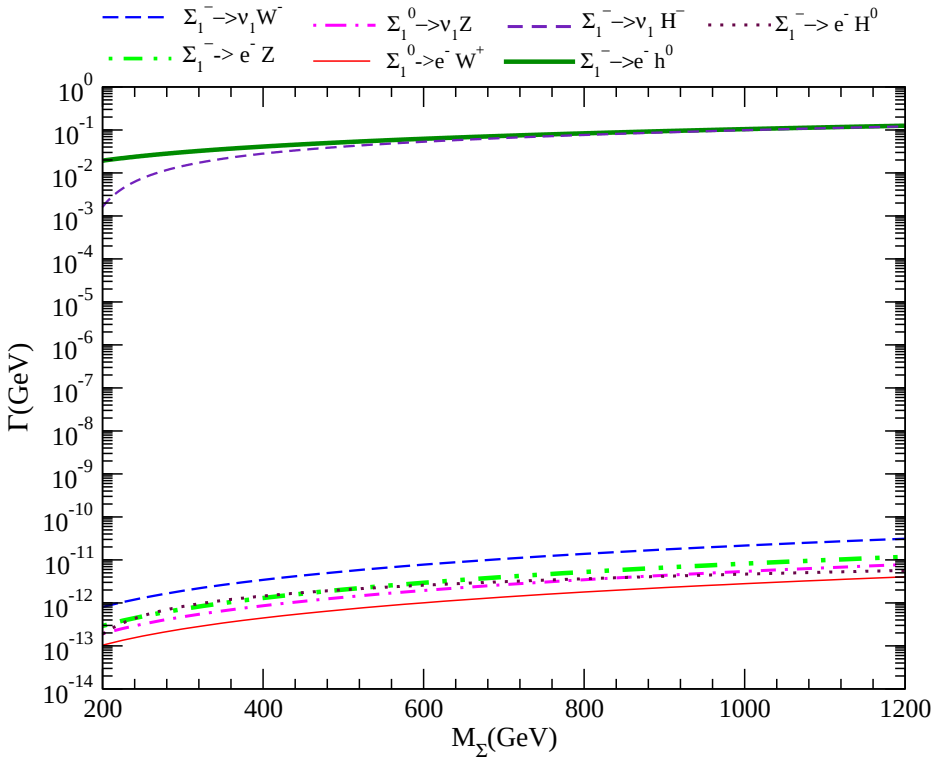

Figure 8: Comparison of the decay rate of the heavy fermion into (i) Higgs and (ii) vector bosons, in our two Higgs doublet model.

$\Sigma_1^- \to e^- H^0$ (dotted maroon line), $\Sigma_1^- \to \nu_1 H^-$ (dashed violet line), and $\Sigma_1^- \to e^- h^0$ (thick solid dark green line). One can clearly see that all decays to gauge bosons are suppressed with respect to decays to h^0 (and A^0) and $H^\pm$ by a factor of more than 10^{10}. The reason for this can be seen by comparing the vertex factors involved in decays to Higgs h^0, A^0 and $H^\pm$ (cf. Eqs. (56), (59), (60), (61), (62)), with decays to gauge bosons (cf. Eqs. (64) and (65)). It is clear that while the former vertex factors do not have any suppression factor, the latter are all suppressed by v'/M_Σ. Another important difference between the decay rates to Higgs given in Eq. (53), and gauge bosons given in Eq. (63), is in the kinematic factors. Comparison of the two equations reveals that (for $m_l = 0$), there is an additional factor of $(2+M_\Sigma^2/M_V^2)$ for the gauge boson decays. This extra M_Σ^2 in the numerator cancels out the $1/M_\Sigma^2$ in the denominator coming from the square of the vertex factors. However, the suppression of the gauge boson decay rates due to $g^2 v'^2/M_V^2 \propto v'^2/V^2$ remains, where $V^2 = v'^2 + v^2$. Since we have taken $v' \sim 10^{-3}$-10^{-4} GeV, the decays to gauge bosons are suppressed by a factor of $\sim 10^{10}$-10^{12} compared to the decays to Higgs. Therefore, branching ratios of the heavy fermion decay to $W^\pm$ and Z can be neglected in our model and we concentrate on only decays to h^0, A^0 and $H^\pm$ in our next section. Note that the decay to H^0 is also suppressed by a factor of 10^{10}-10^{12}, as was also pointed out earlier. We had seen that this suppression is due to $\sin^2\alpha$ coming from the vertex factor for this

process. Since $\sin^2\alpha \sim 10^{-12}$, we find that the decay rate for this case is of the same order of magnitude as the decays to the gauge bosons. Hence, this is also neglected henceforth.

5.4 Comparison Between One and Two Higgs Doublet Models

It is pertinent to compare the two-body decays of the heavy fermions in our two Higgs doublet model with the usual Type III seesaw models considered earlier which have one Higgs doublet. The expressions for heavy fermion decays to Higgs and gauge bosons in the one Higgs doublet models have been given before in the literature [18–21], and we give them here for the sake of comparison. The decay rates to gauge bosons in the one Higgs doublet model is given as (for $m_l = 0$)

$$\Gamma^{1HDM}(\Sigma^0 \to \nu Z) \simeq \frac{\lambda^2 M_\Sigma}{64\pi}(1 - \frac{M_Z^2}{{M_\Sigma}^2})^2(1 + 2\frac{M_Z^2}{{M_\Sigma}^2}), \tag{66}$$

$$\Gamma^{1HDM}(\Sigma^0 \to l^\mp W^\pm) \simeq \frac{\lambda^2 M_\Sigma}{32\pi}(1 - \frac{M_W^2}{{M_\Sigma}^2})^2(1 + 2\frac{M_W^2}{{M_\Sigma}^2}), \tag{67}$$

$$\Gamma^{1HDM}(\Sigma^\pm \to l^\pm Z) \simeq \frac{\lambda^2 M_\Sigma}{32\pi}(1 - \frac{M_Z^2}{{M_\Sigma}^2})^2(1 + 2\frac{M_Z^2}{{M_\Sigma}^2}), \tag{68}$$

$$\Gamma^{1HDM}(\Sigma^\pm \to \nu W^\pm) \simeq \frac{\lambda^2 M_\Sigma}{16\pi}(1 - \frac{M_Z^2}{{M_\Sigma}^2})^2(1 + 2\frac{M_Z^2}{{M_\Sigma}^2}). \tag{69}$$

where λ is the triplet fermion – lepton doublet – Higgs doublet Yukawa coupling in the one Higgs doublet model, and all mixing terms are neglected. This should be compared with the corresponding expression given in Eq. (63), which on neglecting all mixing and hence flavor effects reduces to (for $m_l = 0$)

$$\Gamma^{2HDM}(\Sigma^0 \to \nu Z) \simeq \frac{y_\Sigma^2 M_\Sigma}{64\pi}\frac{v'^2}{V^2}(1 - \frac{M_Z^2}{{M_\Sigma}^2})^2(1 + 2\frac{M_Z^2}{{M_\Sigma}^2}), \tag{70}$$

$$\Gamma^{2HDM}(\Sigma^0 \to l^\mp W^\pm) \simeq \frac{y_\Sigma^2 M_\Sigma}{32\pi}\frac{v'^2}{V^2}(1 - \frac{M_W^2}{{M_\Sigma}^2})^2(1 + 2\frac{M_W^2}{{M_\Sigma}^2}), \tag{71}$$

$$\Gamma^{2HDM}(\Sigma^\pm \to l^\pm Z) \simeq \frac{y_\Sigma^2 M_\Sigma}{32\pi}\frac{v'^2}{V^2}(1 - \frac{M_Z^2}{{M_\Sigma}^2})^2(1 + 2\frac{M_Z^2}{{M_\Sigma}^2}), \tag{72}$$

$$\Gamma^{2HDM}(\Sigma^\pm \to \nu W^\pm) \simeq \frac{y_\Sigma^2 M_\Sigma}{16\pi}\frac{v'^2}{V^2}(1 - \frac{M_Z^2}{{M_\Sigma}^2})^2(1 + 2\frac{M_Z^2}{{M_\Sigma}^2}). \tag{73}$$

where $V^2 = v^2 + v'^2$ is the electroweak breaking scale. The scale of the Yukawa coupling constants and VEVs are fixed by the neutrino mass $m_\nu \sim \lambda^2 V^2/M_\Sigma$ for the one Higgs doublet model and $m_\nu \sim y_\Sigma^2 v'^2/M_\Sigma$. If one replaces λ^2 and $y_\Sigma^2 v'^2/V^2$ with $m_\nu M_\Sigma/V^2$ in both set of expressions, one can see that the the decay rates of heavy fermions into gauge bosons are identical for both models.

The rates for decay into Higgs for the one Higgs doublet model neglecting flavor effects, is

given by (for $m_l = 0$)

$$\Gamma^{1HDM}(\Sigma^0 \to \nu H^0) \simeq \frac{\lambda^2 M_\Sigma}{64\pi}(1 - \frac{M_H^2}{{M_\Sigma}^2})^2, \tag{74}$$

$$\Gamma^{1HDM}(\Sigma^\pm \to l^\pm H^0) \simeq \frac{\lambda^2 M_\Sigma}{32\pi}(1 - \frac{M_H^2}{{M_\Sigma}^2})^2. \tag{75}$$

For the two Higgs doublet model, the corresponding decay rates are given by Eq. (53), which on neglecting all flavor effects reduces to (for $m_l = 0$)

$$\Gamma^{2HDM}(\Sigma^0 \to \nu h^0/A^0) \simeq \frac{y_\Sigma^2 \cos^2\alpha\, M_\Sigma}{64\pi}(1 - \frac{M_{h/A}^2}{{M_\Sigma}^2})^2, \tag{76}$$

$$\Gamma^{2HDM}(\Sigma^\pm \to l^\pm h^0/A^0) \simeq \frac{y_\Sigma^2 \cos^2\alpha\, M_\Sigma}{32\pi}(1 - \frac{M_{h/A}^2}{{M_\Sigma}^2})^2, \tag{77}$$

$$\Gamma^{2HDM}(\Sigma^0 \to \nu H^0) \simeq \frac{y_\Sigma^2 \sin^2\alpha\, M_\Sigma}{64\pi}(1 - \frac{M_H^2}{{M_\Sigma}^2})^2, \tag{78}$$

$$\Gamma^{2HDM}(\Sigma^\pm \to l^\pm H^0) \simeq \frac{y_\Sigma^2 \sin^2\alpha\, M_\Sigma}{32\pi}(1 - \frac{M_H^2}{{M_\Sigma}^2})^2, \tag{79}$$

where the first two expressions are for decays to h^0 or A^0 and the last two for decays to H^0. Again, for the same value of $M_\Sigma \sim 100$ GeV in both models, one requires $\lambda \sim 10^{-5}$-10^{-6} for the one Higgs doublet model in order to produce $m_\nu \sim 0.1$ eV, while $y_\Sigma \sim 1$ for our two Higgs doublet model. Therefore, clearly

$$\Gamma^{2HDM}(\Sigma^0 \to \nu h^0/A^0) \sim 10^{11} \times \Gamma^{1HDM}(\Sigma^0 \to \nu H^0),$$

$$\Gamma^{2HDM}(\Sigma^\pm \to l^\pm h^0/A^0) \sim 10^{11} \times \Gamma^{1HDM}(\Sigma^\pm \to l^\pm H^0).$$

Hence, the the exotic fermions decay about 10^{11} times faster in our model compared to the one Higgs doublet model[7]. This could lead to observational consequences at LHC. In particular, authors of [19] talk about using "displaced vertices" as a signature of the Type III seesaw mechanism. In our model the lifetime of the exotic fermions is a factor of 10^{11} shorter and so will be the gap between their primary production vertex and the decay vertex. Our model therefore predicts no displaced vertex for the heavy fermion decays. In addition, decay to h^0 are predominant. The h^0 decay predominantly into $b\bar{b}$ pairs, but with a very long lifetime, as we will discuss in section 6. This will give a distinctive signature of our model at LHC. We will discuss displaced vertices from h^0 decay in section 7.

5.5 Flavor Structure and the Decay Branching Ratios

Finally, we present the branching fractions of the heavy fermion decays. Table 2 shows the branching fractions for the $\Sigma^\pm$, while Table 3 gives the branching fraction for Σ^0 decays.

[7]We reiterate that the decays $\Sigma^0 \to \nu H^0$ and $\Sigma^\pm \to l^\pm H^0$ are suppressed by the $\sin^2\alpha \sim 10^{-12}$ factor and hence turn out to be comparable to the decay rates in the one Higgs doublet model. However, the branching ratio to this mode is negligible and can be neglected.

Decay modes	$\Sigma_1^\pm$	$\Sigma_2^\pm$	$\Sigma_3^\pm$
$\nu\, H^\pm$	0.363	0.473	0.473
$e^\pm\, A^0$	0.247	2.28×10^{-6}	0.0
$\mu^\pm\, A^0$	2.3×10^{-6}	0.125	0.125
$\tau^\pm\, A^0$	2.3×10^{-6}	0.125	0.125
$e^\pm\, h^0$	0.389	2.5×10^{-6}	0.0
$\mu^\pm\, h^0$	3.6×10^{-6}	0.139	0.139
$\tau^\pm\, h^0$	3.6×10^{-6}	0.139	0.139

Table 2: Decay branching fractions of $\Sigma_1^\pm$, $\Sigma_2^\pm$ and $\Sigma_3^\pm$ for M_{h^0}=40, M_{H^0}=150, $M_{H^\pm} = 170$ GeV and $M_{A^0} = 140$ GeV. We have taken model parameters $M_1 = 300$ GeV and $M_2 = M_3 = 600$ GeV.

Decay modes	Σ_1^0	Σ_2^0	Σ_3^0
$e^\mp\, H^\pm$	0.368	4.3×10^{-6}	0.0
$\mu^\mp\, H^\pm$	3.4×10^{-8}	0.236	0.236
$\tau^\mp\, H^\pm$	3.4×10^{-8}	0.236	0.236
$\nu\, A^0$	0.243	0.250	0.250
$\nu\, h^0$	0.386	0.277	0.277

Table 3: Decay branching fractions of Σ_1^0, Σ_2^0 and Σ_3^0 for M_{h^0}=40, M_{H^0}=150, $M_{H^\pm} = 170$ GeV and $M_A = 140$ GeV. We have taken model parameters $M_1 = 300$ GeV and $M_2 = M_3 = 600$ GeV.

For the channels with neutrino in the final state, we give the sum of the branching fraction into all the three generations, as observationally it will be impossible to see the neutrino generations at LHC. We do not show decays to gauge bosons and H^0 as they are suppressed by a factor of 10^{11} with respect to the decays into h^0, A^0 and $H^\pm$. As a result of the inherent μ-τ symmetry in the model, $\Sigma_3^{\pm/0}$ decays to electrons is strictly forbidden and branching ratios of their decay into μ and τ leptons are equal. We find that due to the form of U_{22}, S_{22} and T_{22} given in Eqs. (50), (51) and (52), $\Sigma_2^{\pm/0}$ decays to electrons is also negligible and their probability to decay into μ and τ leptons is equal. We also find that the branching fractions of $\Sigma_2^\pm$ is equal to the branching fractions of $\Sigma_3^\pm$, and similarly for the neutral heavy fermions. We also notice that $\Sigma_1^{\pm/0}$ decays only to electrons and their decay to μ and τ lepton is almost zero. This as pointed out before, comes due to the constraint on the Yukawa couplings from the low energy neutrino oscillation data. The difference between the branching fraction to h^0, A^0 and $H^\pm$ is mainly driven by the difference in the masses which we have chosen for these Higgses.

6 Higgs Decay

In the previous section we concluded that the heavy fermions will all decay into h^0, A^0 or $H^\pm$. We next turn to the subsequent decay of these Higgs particles. We concentrate on the possible decay modes of h^0, A^0 and $H^\pm$ and tabulate only those few which have significant branching ratios. The branching ratios obviously depend on our choice for the Higgs masses as well as our choice of the mixing angles α and β, which appear in the coupling. The part of the Lagrangian containing the interaction terms of the Higgs with the leptons and quarks are given in Appendix B. The interaction of Higgs fields with the gauge fields comes from the Higgs kinetic terms and is the same as the general two Higgs doublet model. Possible decay channels for the charged Higgs involve the $W^\pm$ and the neutral CP even Higgs. It is well known that in the two Higgs doublet model, the $W^\pm - H^\mp - H^0$ coupling is proportional to $\sin(\beta-\alpha)$, whereas $W^\pm - H^\mp - h^0$ coupling is proportional to $\cos(\beta-\alpha)$ [23]. In Appendix A, we have shown how constraint from neutrino mass drives $\sin\alpha \sim \sin\beta \sim 10^{-6}$. Therefore, in our model $H^\pm \to W^\pm H^0$ is always suppressed, irrespective of the Higgs mass[8]. In fact, the only decay channel possible for the charged Higgs in our model is $H^\pm \to W^\pm h^0$, for which the decay branching fraction

$$BR(H^\pm \to W^\pm h^0) = 1.0. \tag{80}$$

The $W^\pm$ next decay into either qq' pairs or $l^\pm\nu_l/\bar{\nu}_l$ pairs with the following decay branching fractions

$$\begin{aligned} BR(W^\pm \to qq') &= 0.67, \\ BR(W^\pm \to e^\pm\nu_e/\bar{\nu}_e) &= 0.11, \\ BR(W^\pm \to \mu^\pm\nu_\mu/\bar{\nu}_\mu) &= 0.11, \\ BR(W^\pm \to \tau^\pm\nu_\tau/\nu_\tau) &= 0.11. \end{aligned} \tag{81}$$

The branching fractions of the neutral Higgs h^0, H^0 and A^0 are given in Table 4. Though H^0 is almost never produced through heavy fermion decays in our model, we have included them in the table for completeness. We find that the neutral Higgs decay to $b\bar{b}$ pairs almost 90% of the times. The second largest decay fraction is to $\tau\bar{\tau}$ pairs, while decays to $c\bar{c}$ happens less than few percent of the times. In our following sections where we look for collider signatures, we will consider h^0 (and A^0) decays to only $b\bar{b}$ and $\tau\bar{\tau}$ pairs.

Finally, a short discussion on direct production of h^0, without involving the heavy fermion decays, is in order. In our model, the lightest Higgs has a mass as low as 40 GeV. This might appear to be a cause of concern, given that such a Higgs was not observed at LEP. However, it is easy to see that this Higgs mass is not excluded by the direct Higgs searches at LEP-2. This is because the coupling corresponding to $Z - Z - h^0$ vertex is given by $(gM_Z/\cos\theta_w)\sin(\beta-\alpha)$. Since in our model $\sin(\beta-\alpha)$ is almost zero, the LEP-2 bound on Higgs mass does not pose any serious threat to our model, irrespective of the mass of h^0.

[8]One can see that this channel is also kinematically forbidden for our choice of the Higgs masses, whereby with $M_{H^\pm} = 170$, it is impossible to create an on-shell pair of $W^\pm$ and H^0.

Decay modes	h^0	H^0	A^0
$b\bar{b}$	0.89	0.87	0.87
$\tau\bar{\tau}$	0.07	0.09	0.09
$c\bar{c}$	0.04	0.04	0.04

Table 4: Decay branching fractions of h^0, H^0 and A^0 for $M_{h^0} = 40$ GeV, $M_{H^0} = 150$ GeV, and $M_{A^0} = 140$ GeV.

7 Displaced h^0 Decay Vertex

Amongst the most significant difference of our model with the usual Type III seesaw model are the decay lifetimes of the heavy fermions and h^0 (as well as A^0). We had seen in section 5 that the total decay rate for 300 GeV Σ^0 is about 4×10^{-2} GeV. This gives the corresponding rest frame lifetime as 4.97×10^{-13} cm. The lifetime for $\Sigma^{\pm}$ is similar. One can check that for the usual one Higgs doublet models, the rest frame lifetime for the heavy fermions is $\simeq 0.5$ cm for $m_\nu = 0.1$ eV and $M_\Sigma \sim 100$ GeV, which is rather large. The authors of [19] therefore proposed that the displaced decay vertex of heavy fermion could be a typical signature of the one Higgs Type III seesaw model. Clearly, for our model with two Higgs doublets, the decay lifetime is 10^{11} times smaller and hence we predict no displaced vertex for the heavy fermion decay. This can be used as a distinguishing signature between the two models.

Another very important and unique feature of our model is the very long lifetime of our neutral Higgs h^0, which comes due to the smallness of $\sin\alpha$. In fact, since $\sin\alpha \sim 10^{-6}$, the lifetime for h^0 in our model is 10^{12} times larger compared to the standard model Higgs. In particular, the h^0 total decay rate is 4×10^{-15} GeV. This gives h^0 a rest frame lifetime of 4.97 cm. For a h^0 with 200 GeV of energy, the lifetime in the lab frame is seen to be close to 25 cm. Therefore, we expect a big gap between the decay vertices of the heavy fermion and the h^0. This displaced h^0 decay vertex should be detectable at the LHC detectors ATLAS and CMS.

We would like to make just a few qualitative remarks about the prospects of detecting the displaced h^0 vertex. Like stressed many times before, the h^0 decay predominantly into $b\bar{b}$ pairs. While b-tagging is a very important and standard tool for collider experiments, and while both ATLAS [34] and CMS [35] have been developing algorithms for tagging the b, there is an additional complication with b-tagging in our model which should be pointed out here. Since the h^0 lifetime is a few 10s of cm in the lab frame, it is expected to decay inside the silicon tracker of ATLAS and CMS. In particular, the pixel tracker of CMS and ATLAS which are only few cm from the center of the beam pipe, will miss the h^0 decay vertex. However, the silicon strip trackers would be useful in observing the b-jets. The tracks from the primary and secondary vertices of the b-hadron should be seen. In addition, one could use the two other standard tools for tagging the b-jets. Firstly, one could the tag the lepton in the jet coming from the semi-leptonic decays of the b-hadron.

These leptons are expected to have smaller p_T compared to the ones coming from $W^\pm$ and Z decays, and hence this is called soft-lepton tagging [34,35]. More importantly, one could construct the invariant mass distribution of the 2 b-jets. This should give us a sharp peak corresponding to the h^0. We therefore expect that ATLAS and CMS should be able to detect the displaced h^0 decay vertex. This would give a characteristic and unambiguous signal of our model.

Note that while the lifetime of h^0 is constrained to be large due to the smallness of $\sin\alpha$ alone in our model, things are slightly more complicated for the lifetime of A^0. This is because in principle A^0 could decay through the mode $A^0 \to Zh^0$. While this is forbidden kinematically for the A^0 mass we assume, one could argue that for a large enough mass for A^0, the lifetime of A^0 could be shorter. However, we stress that even if A^0 decays fast into h^0, that would still produce a displaced vertex, since the h^0 would still have a very long lifetime.

8 Model Signatures at the LHC

Having discussed in details the production and subsequent decays of the exotic fermions, as well as the decay branching fractions of the intermediate Higgs into final state particles, we next describe the signatures of the two Higgs doublet Type III seesaw model at the LHC. We will present a comprehensive list of final state particles and their corresponding collider signatures.

The most important characteristics of our model are the following:

1. Presence of μ-τ symmetry in Y_Σ and M. This is expected to show-up in the flavor of the final state lepton coming directly from the $\Sigma^{\pm/0}$ decay vertex.

2. Presence of two CP even neutral Higgses (h^0 and H^0), one CP odd neutral Higgs (A^0), and a pair of charged Higgs ($H^\pm$).

3. Predominant decay of the heavy fermions into light leptons, and h^0, A^0 or $H^\pm$. Decays into H^0 and gauge bosons almost never happen.

4. Very short lifetime for the heavy fermion due to the very large Yukawa couplings.

5. Predominant decay of h^0 and A^0 into $b\bar{b}$ pairs 89% and 87% of the time, respectively. They decay also into $\tau\bar{\tau}$ 7-9% of the time.

6. Very large lifetime of h^0 and A^0.

7. The Higgs $H^\pm$ decays into $W^\pm h^0$ and almost never into $W^\pm H^0$.

8. Short predicted lifetime for $H^\pm$.

In what follows, we will use these model characteristics to identify distinctive final state channels at the collider. We identify *all* possible channels in the collider for our model

and calculate the respective effective cross-sections. The results are given in Tables 5, 6 and 7. We will also discuss some of the most important channels and the characteristic backgrounds, if any, associated with them. In this section we have only given results for effective cross-sections for the decay of $\Sigma_1^{\pm/0}$ with $M_{\Sigma_1} = 300$ GeV. Results for the other heavy fermion generations can be similarly obtained.

8.1 Signatures from $\Sigma^+\Sigma^-$ decays

We give in Table 5 all possible collider signatures coming from the decay of $\Sigma^+\Sigma^-$ pairs, for our two Higgs doublet Type III seesaw model. In the last column we also give the corresponding effective cross-sections for these channels in units of fb. Of course the final cross-sections can be obtained only after putting in the various cuts and efficiency factors. These efficiency factors will have to be folded with the cross-sections given in Table 5 to get the final effective cross-sections for the various channels. Few clarifications on our notation is in order. Light charged leptons could be released in the final state through two ways: (i) from the decay of the heavy fermions $\Sigma^\pm \to l^\pm h^0$ and $\Sigma^0 \to l^\pm H^\mp$, (ii) from the decays of $W \to l\bar{\nu}_l$. The charged leptons released from the $\Sigma^{\pm/0}$ decays are different from those from $W^\pm$ in two respects. Firstly, the former carry the information on the flavor structure of the model as discussed in the previous sections, while the latter do not. Secondly, since they come from decays of the heavier $\Sigma^{\pm/0}$, they are expected to be harder than the ones from $W^\pm$ decays. We refer to the charged leptons from the $\Sigma^{\pm/0}$ decays as l and the ones from $W^\pm$ decays as l'. The notation OSD stands for opposite sign dileptons from $\Sigma^{\pm/0}$ decays, while OSD' stands for opposite sign dileptons from $W^\pm$ decays. When we have one charged lepton from $\Sigma^{\pm/0}$ decay and an opposite sign charged lepton from $W^\pm$ decay, then it is denoted as $OSD(l + l')$ and so on. [9]

While we provide an exhaustive list of channels for the $\Sigma^+\Sigma^-$ decay mode in Table 5, obviously not all of them can be effectively used at the LHC to provide smoking gun evidence for our two-Higgs doublet Type III seesaw model. We will highlight below a few of these channels which appear to be particularly promising.

- As discussed in details before, one of the main decay channels of $\Sigma^\pm$ is $\Sigma^\pm \to l^\pm\, h^0$. The h^0 with mass of 40 GeV, then decays subsequently to $b\bar{b}$ pairs giving rise to a final state signal of a pair of opposite sign dileptons (OSD) + 4 b-jets.

  $$\Sigma^+\Sigma^- \to l^+l^- h^0 h^0 \to l^+l^- b\bar{b}b\bar{b} \to 4b + OSD.$$

  We have seen from Table 2 that the branching ratio for $\Sigma^\pm \to l^\pm\, A^0$ is also comparable. This will also produce the same collider signature of $4b + OSD$. The only observable difference will be that the b-jets produced from the A^0 decay will be harder

[9] We should also mention at this point that for some cases whether the charged lepton in the final state is a l or l' can be said from the detector topology only after proper cuts have been imposed on the lepton transverse momentum. This will however require detailed simulation, which is outside the scope of this paper and will be done in an independent work.

Sl no	Channels	Effective cross-section (in fb)
1	$\Sigma^+\Sigma^- \to l^+l^-h^0h^0 \to 4b + OSD$	35.84
2	$\Sigma^+\Sigma^- \to l^+l^-h^0h^0 \to 2b + OSD + 2\tau$	3.67
3	$\Sigma^+\Sigma^- \to l^+l^-h^0h^0 \to OSD + 4\tau$	0.37
4	$\Sigma^+\Sigma^- \to l^+h^0H^-\nu \to 4b + l + 2j + \not{p}_T$	26.88
5	$\Sigma^+\Sigma^- \to l^+h^0H^-\nu \to 4b + OSD(l + l') + \not{p}_T$	8.92
6	$\Sigma^+\Sigma^- \to l^+h^0H^-\nu \to 4b + l + \tau + \not{p}_T$	4.48
7	$\Sigma^+\Sigma^- \to l^+h^0H^-\nu \to 2b + l + 2\tau + 2j + \not{p}_T$	2.69
8	$\Sigma^+\Sigma^- \to l^+h^0H^-\nu \to 2b + l + 3\tau + \not{p}_T$	0.45
9	$\Sigma^+\Sigma^- \to l^+h^0H^-\nu \to 2b + OSD(l + l') + 2\tau + \not{p}_T$	0.9
10	$\Sigma^+\Sigma^- \to l^+h^0H^-\nu \to l + 4\tau + 2j + \not{p}_T$	0.28
11	$\Sigma^+\Sigma^- \to l^+h^0H^-\nu \to OSD(l + l') + 4\tau + \not{p}_T$	0.04
12	$\Sigma^+\Sigma^- \to l^+h^0H^-\nu \to l + 5\tau + \not{p}_T$	0.02
13	$\Sigma^+\Sigma^- \to H^+\nu H^-\nu \to 4b + 4j + \not{p}_T$	15.68
14	$\Sigma^+\Sigma^- \to H^+\nu H^-\nu \to 4b + 2j + l' + \not{p}_T$	10.52
15	$\Sigma^+\Sigma^- \to H^+\nu H^-\nu \to 4b + 2j + \tau + \not{p}_T$	5.26
16	$\Sigma^+\Sigma^- \to H^+\nu H^-\nu \to 4b + OSD' + \not{p}_T$	0.86
17	$\Sigma^+\Sigma^- \to H^+\nu H^-\nu \to 4b + 2\tau + \not{p}_T$	0.43
18	$\Sigma^+\Sigma^- \to H^+\nu H^-\nu \to 4b + 1\tau + 1l' + \not{p}_T$	0.53
19	$\Sigma^+\Sigma^- \to H^+\nu H^-\nu \to 2b + 2\tau + 4j + \not{p}_T$	3.25
20	$\Sigma^+\Sigma^- \to H^+\nu H^-\nu \to 2b + 2\tau + 2j + l' + \not{p}_T$	2.12
21	$\Sigma^+\Sigma^- \to H^+\nu H^-\nu \to 2b + 3\tau + 2j + \not{p}_T$	1.06
22	$\Sigma^+\Sigma^- \to H^+\nu H^-\nu \to 2b + 2\tau + OSD' + \not{p}_T$	0.32
23	$\Sigma^+\Sigma^- \to H^+\nu H^-\nu \to 2b + 4\tau + \not{p}_T$	0.08
24	$\Sigma^+\Sigma^- \to H^+\nu H^-\nu \to 2b + 3\tau + l' + \not{p}_T$	0.02
25	$\Sigma^+\Sigma^- \to H^+\nu H^-\nu \to 4\tau + 4j + \not{p}_T$	0.15
26	$\Sigma^+\Sigma^- \to H^+\nu H^-\nu \to 4\tau + 2j + l' + \not{p}_T$	0.10
27	$\Sigma^+\Sigma^- \to H^+\nu H^-\nu \to 5\tau + 2j + \not{p}_T$	0.05
28	$\Sigma^+\Sigma^- \to H^+\nu H^-\nu \to 5\tau + l' + \not{p}_T$	0.006
29	$\Sigma^+\Sigma^- \to H^+\nu H^-\nu \to 4\tau + OSD' + \not{p}_T$	0.02
30	$\Sigma^+\Sigma^- \to H^+\nu H^-\nu \to 6\tau + \not{p}_T$	0.005

Table 5: Effective cross-sections (in fb) for different $\Sigma^+\Sigma^-$ decay channels for $M_{\Sigma_1} = 300$ GeV.

as A^0 is much more massive than h^0. Here and everywhere else in this section, we will ignore the information on the hardness of the b-jets and present the sum of the cross-sections with h^0 and A^0 in the intermediate state. We should also stress that while we write only h^0 explicitly in the intermediate channels in the Tables, the cross-sections given in the final column always also include A^0 as well as h^0. One finds that the effective cross-section for this channel is 35.84 fb, which is rather high. The OSD released are expected to be hard, as they come from the decay of the massive fermions.

Instead of decaying into $b\bar{b}$ pair, the h^0s could decay into $\tau\bar{\tau}$. If one of the h^0 decays into $b\bar{b}$ and the other into $\tau\bar{\tau}$, we will get

$$\Sigma^+\Sigma^- \to l^+l^-h^0h^0 \to l^+l^-b\bar{b}\tau\bar{\tau} \to 2b + OSD + 2\tau.$$

This has an effective cross-section of 3.67 fb, which will reduce further due to the lower τ detection efficiency. A third possibility exists where both the h^0 decay into $\tau\bar{\tau}$ pairs. The effective cross-section for this channel is small as can be seen from the Table 5, and will get smaller once the τ detection efficiencies are folded.

- The other dominant decay channel for $\Sigma^\pm$ decay is $\Sigma^\pm \to \nu H^\pm$. The neutrino will give missing energy while $H^\pm$ will decay into $H^\pm \to W^\pm h^0$. The $W^\pm$ could decay hadronically giving 2 jets or leptonically giving either a τ-jet + missing energy or e/μ lepton + missing energy. Since the lepton released in the $\Sigma^\pm \to l^\pm h^0$ is important both for understanding the flavor structure of the mixing matrix as well as for tagging the channel in order to reduce the background, we consider first the case where one of heavy charged fermion decays into a hard charged lepton and h^0 and the other into a neutrino and $H^\pm$. The most interesting channels in this case turn out to be:

$$\Sigma^+\Sigma^- \to l^+h^0H^-\nu \to l^+h^0h^0W^-\nu \to 4b + l + 2j + \not{p}_T,$$

$$\Sigma^+\Sigma^- \to l^+h^0H^-\nu \to l^+h^0h^0W^-\nu \to 4b + l + \tau + \not{p}_T,$$

where for the former, the two h^0 (one from the Σ^+ decay and another from H^- decay) produce 4 b-jets, and the W^- decays produce two hadronic jets. In the latter channel, the W^- decays into $\tau\nu_\tau$, producing a τ-jet. The effective cross-section for the former channel is 26.88 fb, while that for the latter is 4.48 fb. The effective cross-sections for the other channels with $l^+h^0h^0W^-\nu$ in the intermediate states are given in Table 5. However, their cross-sections are smaller.

- Finally, both the charged heavy fermions could decay through the $H^\pm\nu$ mode. In this case we have the following leading order possibilities:

$$\Sigma^+\Sigma^- \to H^+\nu H^-\nu \to h^0h^0W^+W^-\nu\nu \to 4b + 4j + \not{p}_T,$$

$$\Sigma^+\Sigma^- \to H^+\nu H^-\nu \to h^0h^0W^+W^-\nu\nu \to 4b + 2j + l' + \not{p}_T,$$

$$\Sigma^+\Sigma^- \to H^+\nu H^-\nu \to h^0h^0W^+W^-\nu\nu \to 4b + 2j + \tau + \not{p}_T.$$

The mode $\Sigma^+\Sigma^- \to 4b + OSD' + \not{p}_T$, appearing at serial number 16 in Table 5 could have been easy to tag as it contains 4b-jets and pair of opposite sign dileptons coming from $W^\pm$ decay, and missing energy. However, the effective cross-section for this channel is relatively low. Note that none of the channels with $H^+\nu H^-\nu$ in their intermediate state have l in their final state. For these channels therefore, it is impossible to say anything about the flavor structure of the model.

8.2 $\Sigma^\pm\Sigma^0$ decay

We give in Tables 6 and 7, all possible decay channels, final state configurations of particles, and their corresponding effective cross-sections for the $\Sigma^\pm\Sigma^0$ production and decays. We reiterate that the final effective cross-section after cuts will be obtained once these cross-sections are folded with the efficiency functions. For the leptons we follow the same convention for our notation as done for the previous section.

- We begin by looking at the $\Sigma^\pm\Sigma^0$ decays where $\Sigma^\pm \to l^\pm h^0$ and $\Sigma^0 \to \nu h^0$. This would lead to the following final state configuration

  $$\Sigma^\pm\Sigma^0 \to l^\pm h^0 h^0 \nu \to 4b + l + \not{p}_T,$$

  with a very large effective cross-section of 96.3 fb. This channel should be easy to tag. The 4 hard b-jets come from the displaced h^0 vertices, and the lepton released is hard. This lepton will also carry information on the μ-τ symmetric flavor structure of the model. Another unambiguous channel with significant effective cross-section coming from the $l^\pm h^0 h^0 \nu$ intermediate state is

  $$\Sigma^\pm\Sigma^0 \to l^\pm h^0 h^0 \nu \to 2b + l + 2\tau + \not{p}_T,$$

  where one of the h^0 decays into $\tau\bar{\tau}$.

- The other intermediate state which has very large effective cross-sections is $\Sigma^\pm\Sigma^0 \to \nu H^\pm\, \nu h^0$. The $H^\pm$ would decay into $W^\pm h^0$, and $W^\pm$ into a lepton l' finally giving

  $$\Sigma^\pm\Sigma^0 \to H^\pm \nu h^0 \nu \to 4b + l' + \not{p}_T,$$

  with an effective cross-section of 107.4 fb. Alternatively, the W^- could instead decay into $\tau\bar{\nu}_\tau$ giving

  $$\Sigma^\pm\Sigma^0 \to H^\pm \nu h^0 \nu \to 4b + \tau + \not{p}_T,$$

  with effective cross-section of 53.7 fb, or decay into qq' giving

  $$\Sigma^\pm\Sigma^0 \to H^\pm \nu h^0 \nu \to 4b + 2j + \not{p}_T,$$

  with an effective cross-section of 35.98 fb.

Sl no	Channels	Effective cross-section (in fb)
1	$\Sigma^{\pm}\Sigma^0 \to l^{\pm}h^0h^0\nu \to 4b + l + \not{p}_T$	96.3
2	$\Sigma^{\pm}\Sigma^0 \to l^{\pm}h^0h^0\nu \to 2b + l + 2\tau + \not{p}_T$	19.7
3	$\Sigma^{\pm}\Sigma^0 \to l^{\pm}h^0h^0\nu \to l + 2\tau + \not{p}_T$	0.99
4	$\Sigma^{\pm}\Sigma^0 \to H^{\pm}\nu h^0\nu \to 4b + 1l' + \not{p}_T$	107.4
5	$\Sigma^{\pm}\Sigma^0 \to H^{\pm}\nu h^0\nu \to 4b + \tau + \not{p}_T$	53.7
6	$\Sigma^{\pm}\Sigma^0 \to H^{\pm}\nu h^0\nu \to 4b + 2j + \not{p}_T$	35.98
7	$\Sigma^{\pm}\Sigma^0 \to H^{\pm}\nu h^0\nu \to 2b + 2\tau + 2j + \not{p}_T$	7.36
8	$\Sigma^{\pm}\Sigma^0 \to H^{\pm}\nu h^0\nu \to 2b + 2\tau + l' + \not{p}_T$	2.42
9	$\Sigma^{\pm}\Sigma^0 \to H^{\pm}\nu h^0\nu \to 2b + 3\tau + \not{p}_T$	1.21
10	$\Sigma^{\pm}\Sigma^0 \to H^{\pm}\nu h^0\nu \to 4\tau + 2j + \not{p}_T$	0.38
11	$\Sigma^{\pm}\Sigma^0 \to H^{\pm}\nu h^0\nu \to l' + 4\tau + \not{p}_T$	0.12
12	$\Sigma^{\pm}\Sigma^0 \to H^{\pm}\nu h^0\nu \to 5\tau + \not{p}_T$	0.06
13	$\Sigma^{\pm}\Sigma^0 \to l^{\pm}H^{\mp}l^{\pm}h^0 \to 4b + 2l + 2j$	36.12
14	$\Sigma^{\pm}\Sigma^0 \to l^{\pm}H^{\mp}l^{\pm}h^0 \to 4b + 3l(2l + l') + \not{p}_T$	12.04
15	$\Sigma^{\pm}\Sigma^0 \to l^{\pm}H^{\mp}l^{\pm}h^0 \to 4b + 2l + 1\tau + \not{p}_T$	6.02
16	$\Sigma^{\pm}\Sigma^0 \to l^{\pm}H^{\mp}l^{\pm}h^0 \to 2b + 2l + 2\tau + 2j$	7.4
17	$\Sigma^{\pm}\Sigma^0 \to l^{\pm}H^{\mp}l^{\pm}h^0 \to 2b + 3l(2l + l') + 2\tau + \not{p}_T$	2.4
18	$\Sigma^{\pm}\Sigma^0 \to l^{\pm}H^{\mp}l^{\pm}h^0 \to 2b + 2l + 3\tau + \not{p}_T$	1.20
19	$\Sigma^{\pm}\Sigma^0 \to l^{\pm}H^{\mp}l^{\pm}h^0 \to 2l + 4\tau + 2j$	0.36
20	$\Sigma^{\pm}\Sigma^0 \to l^{\pm}H^{\mp}l^{\pm}h^0 \to 3l(2l + l') + 4\tau + \not{p}_T$	0.12
21	$\Sigma^{\pm}\Sigma^0 \to l^{\pm}H^{\mp}l^{\pm}h^0 \to 2l + 5\tau + \not{p}_T$	0.06

Table 6: Effective cross-sections (in fb) of different $\Sigma^{\pm}\Sigma^0$ decay channels for $M_{\Sigma_1} = 300$ GeV.

Sl no	Channels	Effective cross-section (in fb)
1	$\Sigma^{\pm}\Sigma^{0} \to H^{\pm}\nu H^{\pm}l^{\mp} \to 4b + l + 4j + \not{p}_T$	13.36
2	$\Sigma^{\pm}\Sigma^{0} \to H^{\pm}\nu H^{\pm}l^{\mp} \to 4b + l + \tau + 2j + \not{p}_T$	4.38
3	$\Sigma^{\pm}\Sigma^{0} \to H^{\pm}\nu H^{\pm}l^{\mp} \to 4b + OSD(l + l') + 2j + \not{p}_T$	6.57
4	$\Sigma^{\pm}\Sigma^{0} \to H^{\pm}\nu H^{\pm}l^{\mp} \to 4b + LSD(l + l') + 2j + \not{p}_T$	2.19
5	$\Sigma^{\pm}\Sigma^{0} \to H^{\pm}\nu H^{\pm}l^{\mp} \to 4b + OSD(l + l') + \tau + \not{p}_T$	1.09
6	$\Sigma^{\pm}\Sigma^{0} \to H^{\pm}\nu H^{\pm}l^{\mp} \to 4b + LSD(l + l') + \tau + \not{p}_T$	0.37
7	$\Sigma^{\pm}\Sigma^{0} \to H^{\pm}\nu H^{\pm}l^{\mp} \to 2b + OSD(l + l') + 2\tau + 2j + \not{p}_T$	1.35
8	$\Sigma^{\pm}\Sigma^{0} \to H^{\pm}\nu H^{\pm}l^{\mp} \to 2b + LSD(l + l') + 2\tau + 2j + \not{p}_T$	0.45
9	$\Sigma^{\pm}\Sigma^{0} \to H^{\pm}\nu H^{\pm}l^{\mp} \to 2b + OSD(l + l') + 3\tau + \not{p}_T$	0.23
10	$\Sigma^{\pm}\Sigma^{0} \to H^{\pm}\nu H^{\pm}l^{\mp} \to 2b + LSD(l + l') + 3\tau + \not{p}_T$	0.08
11	$\Sigma^{\pm}\Sigma^{0} \to H^{\pm}\nu H^{\pm}l^{\mp} \to OSD(l + l') + 4\tau + 2j + \not{p}_T$	0.06
12	$\Sigma^{\pm}\Sigma^{0} \to H^{\pm}\nu H^{\pm}l^{\mp} \to LSD(l + l') + 4\tau + 2j + \not{p}_T$	0.02
13	$\Sigma^{\pm}\Sigma^{0} \to H^{\pm}\nu H^{\pm}l^{\mp} \to 2b + l + 2\tau + 4j + \not{p}_T$	2.78
14	$\Sigma^{\pm}\Sigma^{0} \to H^{\pm}\nu H^{\pm}l^{\mp} \to l + 4\tau + 4j + \not{p}_T$	0.14
15	$\Sigma^{\pm}\Sigma^{0} \to H^{\pm}\nu H^{\pm}l^{\mp} \to 4b + 3l(l + 2l') + \not{p}_T$	1.68
16	$\Sigma^{\pm}\Sigma^{0} \to H^{\pm}\nu H^{\pm}l^{\mp} \to 2b + 3l(l + 2l') + 2\tau + \not{p}_T$	0.32
15	$\Sigma^{\pm}\Sigma^{0} \to H^{\pm}\nu H^{\pm}l^{\mp} \to 3l(l + 2l') + 4\tau + \not{p}_T$	0.02
16	$\Sigma^{\pm}\Sigma^{0} \to H^{\pm}\nu H^{\pm}l^{\mp} \to 4b + l + 2\tau + \not{p}_T$	0.42
17	$\Sigma^{\pm}\Sigma^{0} \to H^{\pm}\nu H^{\pm}l^{\mp} \to 2b + l + 4\tau + \not{p}_T$	0.08
18	$\Sigma^{\pm}\Sigma^{0} \to H^{\pm}\nu H^{\pm}l^{\mp} \to l + 5\tau + 2j + \not{p}_T$	0.04
19	$\Sigma^{\pm}\Sigma^{0} \to H^{\pm}\nu H^{\pm}l^{\mp} \to l + 6\tau + \not{p}_T$	0.004
20	$\Sigma^{\pm}\Sigma^{0} \to H^{\pm}\nu H^{\pm}l^{\mp} \to l + l' + 5\tau + \not{p}_T$	0.008

Table 7: Effective cross-sections (in fb) of different $\Sigma^{\pm}\Sigma^{0}$ decay channels for $M_{\Sigma_1} = 300$ GeV.

- Large effective cross-section in the $\Sigma^{\pm}\Sigma^0$ channel is also expected from the following decay chain

$$\Sigma^{\pm}\Sigma^0 \to l^{\pm}h^0 l^{\pm}H^{\mp} \to 4b + 2l + 2j,$$

with effective cross-section of 36.12 fb. Both the leptons in this channel come from the heavy fermion decay vertices and carry the flavor information of the model.

- $\Sigma^{\pm}\Sigma^0$ could also decay through the intermediate states $H^{\pm}\nu H^{\pm}l^{\mp}$. This leads to 20 possible final state particles and collider signatures. These are listed in Table 7. However, the only one which has sizable effective cross-section is

$$\Sigma^{\pm}\Sigma^0 \to l^{\pm}h^0 l^{\pm}H^{\mp} \to 4b + l + 4j + \not{p}_T.$$

However, this channel has 4 light quark jets, which is always prone to problems with backgrounds.

8.3 Backgrounds

Sl no	Channels	Effective cross-section in fb
1	4b +OSD	35.84
2	$4b + l + \not{p}_T$	96.3
3	$4b + l' + \not{p}_T$	107.4
4	$4b + \tau + \not{p}_T$	53.7
5	$4b + l + 2j + \not{p}_T$	26.88
6	$4b + 2l + 2j$	36.12
7	$4b + 3l(2l + l') + \not{p}_T$	12.04

Table 8: Effective cross-sections in fb for $M_{\Sigma_1} = 300$ GeV, for the most important channels for our model.

In Tables 5, 6 and 7 we provided a comprehensive list of collider signature channels for the heavy fermions, and their corresponding effective cross-sections. In the previous subsection we had also discussed some of the most important channels with large effective cross-sections. In Table 8 we give a subset of those highlighted in sections 8.1 and 8.2. These are expected to be the most unambiguous channels, with smallest backgrounds and the largest signal cross-sections. In almost all channels listed in Table 8, the final collider signature contains 4 b-jets and a hard lepton coming from the primary heavy fermion decay vertex. In addition, the 4 b-jets come from the h^0 decay vertex which is significantly

displaced with respect to the heavy fermion decay vertex. The main source of standard model background for the channels with 4 b-jets and a lepton are the $t\bar{t}b\bar{b}$ modes, which can give multiple b-jets, leptons and missing energy. However, as mentioned many times before, the b-jets come from h^0 displaced vertex and should not have any standard model background. Having the hard lepton in the final state further cuts down the background. Therefore, each of these collider channels are expected to have very little to no backgrounds. For a detailed signal to background analysis one requires a detailed simulation for the final state topology, which is outside the scope of this work. Nevertheless we add a few lines discussing qualitatively the possibility of backgrounds for some of the listed channels in Table 8.

- 4b +OSD: Here the two opposite sign dileptons come from the $\Sigma^+\Sigma^-$ decays. Since the $\Sigma^\pm$ are heavy with $M_{\Sigma^\pm} = 300$ GeV, the leptons will be very hard and we can put a cut of $p_T \gtrsim 100$ GeV. The displaced h^0 vertex should remove all backgrounds.

- $4b + l + \not{p}_T$: Here $t\bar{t}b\bar{b}$ does not directly give any background, unless one of the leptons from the final state is missed. However, the p_T cut on the hard lepton and the displaced h^0 vertices should effectively remove any residual background.

- $4b + l' + \not{p}_T$: Here the p_T cut on the lepton cannot be imposed as the lepton here comes from $W^\pm$ decay. However, the 4 b-jets still come from the displaced h^0 vertices and that should anyway take care of killing all backgrounds to a large extent.

- $4b + l + 2jet + \not{p}_T$: The main background could again come from standard model $t\bar{t}b\bar{b}$ channels. This can also be removed by the displaced h^0 vertex and a cut of $p_T \gtrsim 100$ GeV for the lepton.

- $4b + 2l + 2j$: Similar to the first case, but with 2 extra jets.

- $4b + 3l(2l + l') + \not{p}_T$: Out of the 3 leptons in this channel, two are hard and one is relatively soft. In addition we have the h^0 displaced vertex. Therefore, this channel is expected to be absolutely background free.

9 Conclusions

The seesaw mechanism has remained the most elegant scheme to explain the smallness of the neutrino masses without having to unnaturally fine tune the Yukawa couplings to very small values. In the so-called Type III seesaw, three self-conjugate ($Y = 0$) SU(2) triplet fermions are added to the standard model particle content. These exotic fermions are color singlets and belong to the adjoint representation of SU(2). These exotic fermions have Yukawa couplings with the standard model lepton doublet and the Higgs doublet. They also have a Majorana mass term. Once these heavy leptons are integrated out from the theory, we are left with a Majorana mass term for the neutrino given by the famous seesaw formula, where the smallness of the neutrino mass is explained by the largeness of

the heavy fermion mass, without having to fine tune the Yukawa couplings to very small values. To generate neutrino masses $m_\nu \sim 0.1$ eV, one requires that the heavy fermion mass should be $\sim 10^{14}$ GeV. Being in the adjoint representation of SU(2), one of the most interesting feature of these exotic fermions is that they have gauge couplings, and therefore can be produced at collider experiments. The only constraint for the production of these particles at LHC is that their mass should be in a few 100 GeV range. However, in order to produce neutrino masses $m_\nu \sim 0.1$ eV, one would then have to tune the Yukawa couplings to be $\sim 10^{-6}$, which ruins completely the very spirit and motivation for seesaw.

In order to circumvent this problem and preserve the motivation of the seesaw mechanism, we propose an extended Type III seesaw model with two SU(2) Higgs doublets along with the three self-conjugate SU(2) fermion triplets. We impose an additional Z_2 symmetry such that one of the Higgs doublets, called Φ_1, has positive charge while the other, called Φ_2, has negative charge under this symmetry. In addition, we demand that all standard model particles have positive charge with respect to Z_2 while the three new exotic fermion triplets are negatively charged. Therefore, Φ_1 behaves like the standard model Higgs, while Φ_2 is coupled *only* to the exotic fermion triplets. As a result, the neutrino mass term coming from the seesaw formula depends on the VEV of Φ_2 (v'), while all other fermion masses are dependent on the VEV of Φ_1 (v). We can therefore choose a value for v' such that $m_\nu \sim 0.1$ eV for exotic fermion masses ~ 100 GeV, without having to fine tune the Yukawa couplings to very small values.

Another typical feature about neutrinos concern their peculiar mixing pattern which should be explained by the underlying theory. The current neutrino oscillation data suggests an inherent μ-τ symmetry in the low energy neutrino mass matrix. It is therefore expected that this μ-τ symmetry should also exist at the high scale, either on its own or as a sub-group of a bigger flavor group. We imposed an exact μ-τ symmetry on both the Yukawa coupling of the triplet fermions Y_Σ as well as on their Majorana mass matrix M. Therefore the low energy neutrino matrix $\tilde{m}$ obtained after the seesaw had an in-built μ-τ symmetry. As a result our model predicts $\theta_{23} = \pi/4$ and $\theta_{13} = 0$. The mixing angle θ_{12} as well as the mass squared differences Δm^2_{21} and Δm^2_{31} are given in terms of the entries of Y_Σ and M. We showed how the oscillation parameters depend on the model parameters in Y_Σ and M.

A very important and new aspect which emerged from our study concerns the mixing in the heavy fermion sector. It had been assumed in all past studies that the mixing matrices U_Σ, U_h^L and U_h^R which diagonalize the heavy fermion mass matrices $\tilde{M}_\Sigma$, $M_H^\dagger M_H$ and $M_H M_H^\dagger$ respectively, are almost unit matrices. However, we showed that for the case where M was μ-τ symmetric, these matrices were highly non-trivial, and in particular had the last column as $(0, 1/\sqrt{2}, 1/\sqrt{2})$. We showed that this has observable consequences for the heavy fermion decays at the collider. We showed that flavor structure of our model was reflected in the pattern of heavy fermion decays into light charged leptons. These showed a μ-τ symmetry. The state $\Sigma_3^{\pm/0}$ decayed equally into muons and taus and almost never decayed into electrons. We have checked that this feature exists not only for our model, but for any model with an underlying flavor symmetry group that imposes μ-τ symmetry on the heavy Majorana mass matrix M. In fact, we have made explicit checks

on the seesaw model proposed by Altarelli and Feruglio [36], where A_4 was imposed as the flavor symmetry group. Though the proposed A_4 model by Altarelli and Feruglio was a Type I seesaw model, it can be easily adapted to the Type III seesaw case. We found that the mixing matrices U_Σ, U_h^L and U_h^R even for that case had $(0, 1/\sqrt{2}, 1/\sqrt{2})$ as their last column.

Having established the flavor structure of our model, we next turned to the production and detection of heavy fermions at LHC. We discussed quantitatively and in details the cross-section for the heavy fermion production at LHC and their decay rates. While the production cross-sections for our model turned out to be same as that in all earlier calculations done in the context of the one Higgs doublet model, the decay pattern for the heavy fermions in our case was found to be extremely different and unique. The μ-τ permutation symmetry showed up in the flavor pattern of the heavy fermion decays due to the typical last column $(0, 1/\sqrt{2}, 1/\sqrt{2})$ of the matrices U_Σ, U_h^L and U_h^R. We also showed that in our case the decay rate of the heavy fermions was about 10^{11} times larger than that found for the one Higgs doublet model. In fact, the heavy fermion decay rate for our model is 5.8×10^{-2} GeV and 4×10^{-2} GeV for 300 GeV charged and neutral heavy fermions, respectively. Therefore, while for the one Higgs doublet case one could attempt to look for displaced heavy fermion decay vertices, in our case they will decay almost instantaneously. We found that this tremendous decay rate came from the very fast decays of $\Sigma^{\pm/0}$ into light leptons and Higgs h^0, A^0 or $H^\pm$. The very large decay rate was shown to stem from the very large Yukawa couplings in our model. As the Yukawa couplings are a factor of $10^5 - 10^6$ larger in our model, the decay rates which depend on the square of the Yukawa couplings are a factor 10^{10}-10^{12} higher. Decays into H^0 and gauge bosons in our model was shown to be same as in the one Higgs doublet case, and the reason explained.

Another distinctive feature of our model appeared in the pattern of the Higgs decays. We showed that the smallness of the neutrino masses constrained the neutral Higgs mixing angle α to be very small. This resulted in a very small decay rate for the h^0 Higgs. For a mass of $M_{h^0} = 40$ GeV, the h^0 lifetime in the Higgs rest frame comes out to be about 5 cm. This will give a displaced decay vertex in the LHC detectors, ATLAS and CMS. The lifetime for $H^\pm$ turned out to be small.

Finally, we discussed in detail the expected collider signatures for our two Higgs doublet Type III seesaw model with μ-τ symmetry. We tabulated a comprehensive and exhaustive list of all possible collider signature channels for the heavy fermions at LHC. We gave the effective cross-sections for each of these channels. The effective cross-section for some of these channels were seen to be very high. We made a short-list of channels with very high effective cross-section and low background at LHC. This was presented in Table 8. In all the listed channels we have 4 b-jets coming from the decay of two h^0 which have displaced vertices. In addition, all (except one) of them have a hard lepton in the final state coming from the $\Sigma^{\pm/0}$ decay. This lepton in addition to being hard, also carries information on the μ-τ symmetry of our model. These collider signature channels are hence very distinctive of our model and suffer from almost no standard model background.

In conclusion, we proposed a Type III seesaw model with large Yukawa couplings and triplet fermion masses light enough to be produced at the LHC. This could be achieved

through a unique two Higgs doublet model. The very large Yukawa couplings resulted in very fast decays of the heavy fermions, with a decay rate about 10^{11} times faster than obtained in the earlier Type III seesaw models. We imposed a μ-τ symmetry on our model in order to comply with the low energy neutrino oscillation data. This flavor pattern is reflected also in the mixing matrices of the heavy fermions, which are no longer unity, and which have observable consequences for the heavy fermion decays at the LHC. The neutrino mass constrains also the mixing angle of the neutral Higgs to be very small. This nearly forbids the decay of the heavy fermions into the heavier CP even neutral Higgs H^0. Thus they decay almost always into h^0 (and A^0) and $H^\pm$. More importantly, the small neutral Higgs mixing angle increases the lifetime of the h^0. These are expected to live for more than 10 cm at LHC before decaying predominantly into $b\bar{b}$, producing b-jets. This would be seen as a displaced h^0 decay vertex in the detector. We identified collider signature channels at LHC which have very large effective cross-section and almost no standard model background. These could be used to provide smoking gun evidence for our model.

Acknowledgments

The authors wish to thank A. Abada, B. Bajc, S. Bhattacharyya, F. Bonnet, A. Datta, R. Foot, S. Goswami, T. Hambye, A. Ibarra, K. Matchev, B. Mukhopadhyaya, A. Raychaudhuri and A. Sen for discussions and valuable comments. The authors acknowledge the HRI cluster facilities for computation. This work has been supported by the Neutrino Project and the RECAPP Project under the XI Plan of Harish-Chandra Research Institute.

Appendix

A The Scalar Potential and Higgs Spectrum

Our model has two SU(2) complex Higgs doublets Φ_1 and Φ_2, with hypercharge $Y = 1$. The scalar potential can then be written as

$$\begin{aligned} V &= \lambda_1 \left(\Phi_1^\dagger \Phi_1 - v^2\right)^2 + \lambda_2 \left(\Phi_2^\dagger \Phi_2 - v'^2\right)^2 + \lambda_3 \left((\Phi_1^\dagger \Phi_1 - v^2) + (\Phi_2^\dagger \Phi_2 - v'^2)\right)^2 \\ &\quad + \lambda_4 \left((\Phi_1^\dagger \Phi_1)(\Phi_2^\dagger \Phi_2) - (\Phi_1^\dagger \Phi_2)(\Phi_2^\dagger \Phi_1)\right) + \lambda_5 \left(\mathrm{Re}(\Phi_1^\dagger \Phi_2) - v v' \cos\xi\right)^2 \\ &\quad + \lambda_6 \left(\mathrm{Im}(\Phi_1^\dagger \Phi_2) - v v' \sin\xi\right)^2, \end{aligned} \tag{A1}$$

where

$$\langle \Phi_1 \rangle = \begin{pmatrix} 0 \\ v \end{pmatrix}, \quad \langle \Phi_2 \rangle = \begin{pmatrix} 0 \\ v' e^{i\xi} \end{pmatrix}, \quad \text{and} \quad \tan\beta = \frac{v'}{v}. \tag{A2}$$

Recall that under the imposed Z_2 symmetry, Φ_1 carries charge $+1$, while Φ_2 has -1 charge. Therefore, the λ_5 term is zero when the symmetry is exact. We will discuss shortly the

phenomenological consequences of this and argue in favor of a mild breaking of this Z_2 symmetry. With the scalar potential Eq. (A1) it is straightforward to obtain the Higgs mass matrix and obtain the corresponding mass spectrum. The physical degrees of freedoms contain the charged Higgs $H^\pm$ and the neutral Higgs H^0, h^0, and A^0. While H^0 and h^0 are CP even, A^0 is CP odd. If we work in a simplified scenario where ξ is taken as zero, then it is is quite straightforward to derive the mass of the charged Higgs $H^\pm$ and the CP-odd Higgs A^0. The masses are given as

$$M^2_{H^\pm} = \lambda_4(v^2 + v'^2), \quad \text{and} \quad M^2_{A^0} = \lambda_6(v^2 + v'^2), \tag{A3}$$

respectively. The mass matrix for the neutral CP-even Higgs is

$$M' = \begin{pmatrix} 4v^2(\lambda_1 + \lambda_3) + v'^2\lambda_5 & (4\lambda_3 + \lambda_5)vv' \\ (4\lambda_3 + \lambda_5)vv' & 4v'^2(\lambda_2 + \lambda_3) + v^2\lambda_5 \end{pmatrix}. \tag{A4}$$

The mixing angle, obtained from diagonalizing the above matrix is given by

$$\tan 2\alpha = \frac{2\,M_{12}}{M_{11} - M_{22}}, \tag{A5}$$

and the corresponding masses are

$$M^2_{H^0,h^0} = \frac{1}{2}\{M_{11} + M_{22} \pm \sqrt{(M_{11} - M_{22})^2 + 4M^2_{12}}. \tag{A6}$$

The physical Higgs are given in terms of components of Φ_1 and Φ_2 as follows. The neutral Higgs are given as

$$H^0 = \sqrt{2}\left((\mathrm{Re}\Phi^0_1 - v)\cos\alpha + (\mathrm{Re}\Phi^0_2 - v')\sin\alpha\right), \tag{A7}$$

$$h^0 = \sqrt{2}\left(-(\mathrm{Re}\Phi^0_1 - v)\sin\alpha + (\mathrm{Re}\Phi^0_2 - v')\cos\alpha\right), \tag{A8}$$

$$A^0 = \sqrt{2}(-\mathrm{Im}\Phi^0_1\sin\beta + \mathrm{Im}\Phi^0_2\cos\beta), \tag{A9}$$

while the charged Higgs are

$$H^\pm = -\Phi^\pm_1\sin\beta + \Phi^\pm_2\cos\beta. \tag{A10}$$

The Goldstones turn out to be

$$G^\pm = \Phi^\pm_1\cos\beta + \Phi^\pm_2\sin\beta \tag{A11}$$

$$G^0 = \sqrt{2}(\mathrm{Im}\Phi^0_1\cos\beta + \mathrm{Im}\Phi^0_2\sin\beta). \tag{A12}$$

Recall that the requirement from small neutrino masses $m_\nu \sim 0.1$ eV constrains $v' \sim 10^{-4}$ GeV. Therefore, for our model we get from Eqs. (A2) and (A5)

$$\tan\beta \sim 10^{-6}, \quad \text{and} \quad \tan 2\alpha \sim \tan\beta \sim 10^{-6}. \tag{A13}$$

One can estimate from Eq. (A6), that in the limit $v' \ll v$,

$$M^2_{H^0} \simeq (\lambda_1 + \lambda_3)v^2, \quad \text{and} \quad M^2_{h^0} \simeq \lambda_5 v^2. \tag{A14}$$

We should point out here that in the limit of exact Z_2 symmetry, $\lambda_5 = 0$ exactly, and in that case $M^2_{h^0} \propto \frac{{\lambda_3}^2}{(\lambda_1+\lambda_3)^2} v'^2$. Since $v' \sim 10^{-4}$ GeV, this would give a very tiny mass for the neutral Higgs h^0. To prevent that, we introduce a mild explicit breaking of the Z_2 symmetry, by taking $\lambda_5 \neq 0$ in the scalar potential. This not only alleviates the problem of an extremely light Higgs boson, it also circumvents spontaneous breaking of Z_2, when the Higgs develop vacuum expectation value. This saves the model from complications such as creation of domain walls, due to the spontaneous breaking of a discrete symmetry. The extent of breaking of Z_2 is determined by the strength of λ_5. Since we wish to impose only a mild breaking, we take $\lambda_5 \sim 0.05$. This gives us a light neutral Higgs mass of $M^0_h \simeq 40$ GeV from Eq. (A14). Since all other $\lambda_i \sim 1$, the mass of the other CP even neutral Higgs, the CP odd neutral Higgs and the charged Higgs are all seen to be $\sim v$ GeV from Eqs. (A3) and (A14). We will work with $M^0_H = 150$ GeV, $M^0_A = 140$ GeV and $M^\pm_H = 170$ GeV.

Also required are the couplings of our Higgs with the gauge bosons. This is needed in order to understand the Higgs decay and the subsequent collider signatures of our model. These are standard expressions and are well documented (see for instance [23]). One can check that certain couplings depend on $\sin\alpha$ and $\sin(\beta-\alpha)$. From Eq. (A13) we can see that these couplings are almost zero. Others depend on $\cos\alpha$ and $\cos(\beta-\alpha)$ and therefore large. We refer the reader to [23] for a detailed discussion on the general form for the coulings.

B Appendix B: The Interaction Lagrangian

B.1 Lepton-Higgs Coupling

The lepton Yukawa part of the Lagrangian for our two Higgs doublet model was given in Eq. (9) as,

$$-\mathcal{L}_Y = \left[Y_{l_{ij}} \overline{l}'_{R_i} \Phi_1^\dagger L'_j + Y_{\Sigma_{ij}} \tilde{\Phi}_2^\dagger \overline{\Sigma}'_{R_i} L'_j + h.c.\right] + \frac{1}{2} M_{ij} \,\mathrm{Tr}\left[\overline{\Sigma'}_{R_i} \tilde{\Sigma}^C_{R_j} + h.c.\right]. \tag{B1}$$

From this one can extract the individual Yukawa coupling vertex factors between two fermions and a Higgs. We have three generations of heavy and light neutral leptons and three generations of heavy and light charged leptons. In addition, we have three neutral and a pair of charged Higgs. The Yukawa interaction between any pair of fermions and a corresponding physical Higgs field can be extracted from Eq. (B1). We list below all Yukawa possible interactions *in the mass basis* of the particles. The vertex factors are denoted as $C^{X,L/R}_{FI}$, where F and I are the initial and final state fermions respectively, X is the physical Higgs involved and L/R are for either the vertex with P_L or P_R respectively, where P_L and P_R are the left and right chiral projection operators respectively. Note that

we have suppressed the generation indices for clarity of the expressions. But the generation indices are implicitly there and the vertex factors are all 3×3 matrices.

$$
\begin{aligned}
-\mathcal{L}^{H^0}_{l,\Sigma^-} &= H^0\{\bar{l}(C^{H^0,L}_{ll}P_L + C^{H^0,R}_{ll}P_R)l + \{\bar{l}(C^{H^0,L}_{l\Sigma^-}P_L + C^{H^0,R}_{l\Sigma^-}P_R)\Sigma^- + h.c\} \\
&\quad + \overline{\Sigma^-}(C^{H^0,L}_{\Sigma^-\Sigma^-}P_L + C^{H^0,R}_{\Sigma^-\Sigma^-}P_R)\Sigma^-\}
\end{aligned} \tag{B2}
$$

$$
\begin{aligned}
-\mathcal{L}^{h^0}_{l,\Sigma^-} &= h^0\{\bar{l}(C^{h^0,L}_{ll}P_L + C^{h^0,R}_{ll}P_R)l + \{\bar{l}(C^{h^0,L}_{l\Sigma^-}P_L + C^{h^0,R}_{l\Sigma^-}P_R)\Sigma^- + h.c\} \\
&\quad + \overline{\Sigma^-}(C^{h^0,L}_{\Sigma^-\Sigma^-}P_L + C^{h^0,R}_{\Sigma^-\Sigma^-}P_R)\Sigma^-\}
\end{aligned} \tag{B3}
$$

$$
\begin{aligned}
-\mathcal{L}^{A^0}_{l,\Sigma^-} &= A^0\{\bar{l}(C^{A^0,L}_{ll}P_L + C^{A^0,R}_{ll}P_R)l + \{\bar{l}(C^{A^0,L}_{l\Sigma^-}P_L + C^{A^0,R}_{l\Sigma^-}P_R)\Sigma^- + h.c\} \\
&\quad + \overline{\Sigma^-}(C^{A^0,L}_{\Sigma^-\Sigma^-}P_L + C^{A^0,R}_{\Sigma^-\Sigma^-}P_R)\Sigma^-\}
\end{aligned} \tag{B4}
$$

$$
\begin{aligned}
-\mathcal{L}^{G^0}_{l,\Sigma^-} &= G^0\{\bar{l}(C^{G^0,L}_{ll}P_L + C^{G^0,R}_{ll}P_R)l + \{\bar{l}(C^{G^0,L}_{l\Sigma^-}P_L + C^{G^0,R}_{l\Sigma^-}P_R)\Sigma^- + h.c\} \\
&\quad + \overline{\Sigma^-}(C^{G^0,L}_{\Sigma^-\Sigma^-}P_L + C^{G^0,R}_{\Sigma^-\Sigma^-}P_R)\Sigma^-\}
\end{aligned} \tag{B5}
$$

$$
\begin{aligned}
-\mathcal{L}^{H^0}_{\nu,\Sigma^0} &= H^0\{\overline{\nu'}(C^{H^0,L}_{\nu\nu}P_L + C^{H^0,R}_{\nu\nu}P_R)\nu + \{\overline{\nu'}(C^{H^0,L}_{\nu\Sigma^0}P_L + C^{H^0,R}_{\nu\Sigma^0}P_R)\Sigma^0 + h.c\} \\
&\quad + \overline{\Sigma^0}(C^{H^0,L}_{\Sigma^0\Sigma^0}P_L + C^{H^0,R}_{\Sigma^0\Sigma^0}P_R)\Sigma^0\}
\end{aligned} \tag{B6}
$$

$$
\begin{aligned}
-\mathcal{L}^{h^0}_{\nu,\Sigma^0} &= h^0\{\overline{\nu'}(C^{h^0,L}_{\nu\nu}P_L + C^{h^0,R}_{\nu\nu}P_R)\nu + \{\overline{\nu}(C^{h^0,L}_{\nu\Sigma^0}P_L + C^{h^0,R}_{\nu\Sigma^0}P_R)\Sigma^0 + h.c\} \\
&\quad + \overline{\Sigma^0}(C^{h^0,L}_{\Sigma^0\Sigma^0}P_L + C^{h^0,R}_{\Sigma^0\Sigma^0}P_R)\Sigma^0\}
\end{aligned} \tag{B7}
$$

$$
\begin{aligned}
-\mathcal{L}^{A^0}_{\nu,\Sigma^0} &= A^0\{\overline{\nu}(C^{A^0,L}_{\nu\nu}P_L + C^{A^0,R}_{\nu\nu}P_R)\nu + \{\overline{\nu}(C^{A^0,L}_{\nu\Sigma^0}P_L + C^{A^0,R}_{\nu\Sigma^0}P_R)\Sigma^0 + h.c\} \\
&\quad + \overline{\Sigma^0}(C^{A^0,L}_{\Sigma^0\Sigma^0}P_L + C^{A^0,R}_{\Sigma^0\Sigma^0}P_R)\Sigma^0\}
\end{aligned} \tag{B8}
$$

$$
\begin{aligned}
-\mathcal{L}^{G^0}_{\nu,\Sigma^0} &= G^0\{\overline{\nu}(C^{G^0,L}_{\nu\nu}P_L + C^{A^0,R}_{\nu\nu}P_R)\nu + \{\overline{\nu}(C^{G^0,L}_{\nu\Sigma^0}P_L + C^{G^0,R}_{\nu\Sigma^0}P_R)\Sigma^0 + h.c\} \\
&\quad + \overline{\Sigma^0}(C^{G^0,L}_{\Sigma^0\Sigma^0}P_L + C^{G^0,R}_{\Sigma^0\Sigma^0}P_R)\Sigma^0\}
\end{aligned} \tag{B9}
$$

$C_{ll}^{H^0,L}$	$\frac{1}{\sqrt{2}}(T_{11}^\dagger Y_l S_{11}\cos\alpha + T_{21}^\dagger Y_\Sigma S_{11}\sin\alpha)$	$C_{ll}^{H^0,R}$	$\frac{1}{\sqrt{2}}(S_{11}^\dagger Y_l^\dagger T_{11}\cos\alpha + S_{11}^\dagger Y_\Sigma^\dagger T_{21}\sin\alpha)$
$C_{l\Sigma^-}^{H^0,L}$	$\frac{1}{\sqrt{2}}(T_{11}^\dagger Y_l S_{12}\cos\alpha + T_{21}^\dagger Y_\Sigma S_{12}\sin\alpha)$	$C_{l\Sigma^-}^{H^0,R}$	$\frac{1}{\sqrt{2}}(S_{11}^\dagger Y_l^\dagger T_{12}\cos\alpha + S_{11}^\dagger Y_\Sigma^\dagger T_{22}\sin\alpha)$
$C_{\Sigma^-\Sigma^-}^{H^0,L}$	$\frac{1}{\sqrt{2}}(T_{12}^\dagger Y_l S_{12}\cos\alpha + T_{22}^\dagger Y_\Sigma S_{12}\sin\alpha)$	$C_{\Sigma^-\Sigma^-}^{H^0,R}$	$\frac{1}{\sqrt{2}}(S_{12}^\dagger Y_l^\dagger T_{12}\cos\alpha + S_{12}^\dagger Y_\Sigma^\dagger T_{22}\sin\alpha)$
$C_{ll}^{h^0,L}$	$\frac{-1}{\sqrt{2}}(T_{11}^\dagger Y_l S_{11}\sin\alpha - T_{21}^\dagger Y_\Sigma S_{11}\cos\alpha)$	$C_{ll}^{h^0,R}$	$\frac{-1}{\sqrt{2}}(S_{11}^\dagger Y_l^\dagger T_{11}\sin\alpha - S_{11}^\dagger Y_\Sigma^\dagger T_{21}\cos\alpha)$
$C_{l\Sigma^-}^{h^0,L}$	$\frac{-1}{\sqrt{2}}(T_{11}^\dagger Y_l S_{12}\sin\alpha - T_{21}^\dagger Y_\Sigma S_{12}\cos\alpha)$	$C_{l\Sigma^-}^{h^0,R}$	$\frac{-1}{\sqrt{2}}(S_{11}^\dagger Y_l^\dagger T_{12}\sin\alpha - S_{11}^\dagger Y_\Sigma^\dagger T_{22}\cos\alpha)$
$C_{\Sigma^-\Sigma^-}^{h^0,L}$	$\frac{-1}{\sqrt{2}}(T_{12}^\dagger Y_l S_{12}\sin\alpha - T_{22}^\dagger Y_\Sigma S_{12}\cos\alpha)$	$C_{\Sigma^-\Sigma^-}^{h^0,R}$	$\frac{-1}{\sqrt{2}}(S_{12}^\dagger Y_l^\dagger T_{12}\sin\alpha - S_{12}^\dagger Y_\Sigma^\dagger T_{22}\cos\alpha)$
$C_{ll}^{A^0,L}$	$\frac{i}{\sqrt{2}}(T_{11}^\dagger Y_l S_{11}\sin\beta + T_{21}^\dagger Y_\Sigma S_{11}\cos\beta)$	$C_{ll}^{A^0,R}$	$\frac{-i}{\sqrt{2}}(S_{11}^\dagger Y_l^\dagger T_{11}\sin\beta + S_{11}^\dagger Y_\Sigma^\dagger T_{21}\cos\beta)$
$C_{l\Sigma^-}^{A^0,L}$	$\frac{i}{\sqrt{2}}(T_{11}^\dagger Y_l S_{12}\sin\beta + T_{21}^\dagger Y_\Sigma S_{12}\cos\beta)$	$C_{l\Sigma^-}^{A^0,R}$	$\frac{-i}{\sqrt{2}}((S_{11}^\dagger Y_l^\dagger T_{12}\sin\beta + S_{11}^\dagger Y_\Sigma^\dagger T_{22}\cos\beta)$
$C_{\Sigma^-\Sigma^-}^{A^0,L}$	$\frac{i}{\sqrt{2}}(T_{12}^\dagger Y_l S_{12}\sin\beta + T_{22}^\dagger Y_\Sigma S_{12}\cos\beta)$	$C_{\Sigma^-\Sigma^-}^{A^0,R}$	$\frac{-i}{\sqrt{2}}(S_{12}^\dagger Y_l^\dagger T_{12}\sin\beta + S_{12}^\dagger Y_\Sigma^\dagger T_{22}\cos\beta)$
$C_{ll}^{G^0,L}$	$\frac{-i}{\sqrt{2}}(T_{11}^\dagger Y_l S_{11}\cos\beta - T_{21}^\dagger Y_\Sigma S_{11}\sin\beta)$	$C_{ll}^{G^0,R}$	$\frac{i}{\sqrt{2}}(S_{11}^\dagger Y_l^\dagger T_{11}\cos\beta - S_{11}^\dagger Y_\Sigma^\dagger T_{21}\sin\beta)$
$C_{l\Sigma^-}^{G^0,L}$	$\frac{-i}{\sqrt{2}}(T_{11}^\dagger Y_l S_{12}\cos\beta - T_{21}^\dagger Y_\Sigma S_{12}\sin\beta)$	$C_{l\Sigma^-}^{G^0,R}$	$\frac{i}{\sqrt{2}}(S_{11}^\dagger Y_l^\dagger T_{12}\cos\beta - S_{11}^\dagger Y_\Sigma^\dagger T_{22}\sin\beta)$
$C_{\Sigma^-\Sigma^-}^{G^0,L}$	$\frac{-i}{\sqrt{2}}(T_{12}^\dagger Y_l S_{12}\cos\beta - T_{22}^\dagger Y_\Sigma S_{12}\sin\beta)$	$C_{\Sigma^-\Sigma^-}^{G^0,R}$	$\frac{i}{\sqrt{2}}(S_{12}^\dagger Y_l^\dagger T_{12}\cos\beta - S_{12}^\dagger Y_\Sigma^\dagger T_{22}\sin\beta)$

Table 9: The vertex factors for P_L (P_R) and their corresponding exact expression in terms of the Yukawa couplings and mixing matrices are given in the first (third) and second (forth) column respectively. The vertex factors listed here are for Yukawa interactions of the charged leptons with neutral Higgs.

$$
\begin{aligned}
-\mathcal{L}_{l,\Sigma^0,\nu,\Sigma^-}^{H^-} &= H^-\{\overline{l}(C_{l\nu}^{H^-,L}P_L + C_{l\nu}^{H^-,R}P_R)\nu + \overline{l}(C_{l\Sigma^0}^{H^-,L}P_L + C_{l\Sigma^0}^{H^-,R}P_R)\Sigma^0 \\
&\quad + \overline{\Sigma^-}(C_{\Sigma^-\nu}^{H^-,L}P_L + C_{\Sigma^-\nu}^{H^-,R}P_R)\nu + \overline{\Sigma^-}(C_{\Sigma^-\Sigma^0}^{H^-,L}P_L + C_{\Sigma^-\Sigma^0}^{H^-,R}P_R)\Sigma^0\} \\
&\quad + h.c
\end{aligned} \tag{B10}
$$

$$
\begin{aligned}
-\mathcal{L}_{l,\Sigma^0,\nu,\Sigma^-}^{G^-} &= H^-\{\overline{l}(C_{l\nu}^{G^-,L}P_L + C_{l\nu}^{G^-,R}P_R)\nu + \overline{l}(C_{l\Sigma^0}^{G^-,L}P_L + C_{l\Sigma^0}^{G^-,R}P_R)\Sigma^0 \\
&\quad + \overline{\Sigma^-}(C_{\Sigma^-\nu}^{G^-,L}P_L + C_{\Sigma^-\nu}^{G^-,R}P_R)\nu + \overline{\Sigma^-}(C_{\Sigma^-\Sigma^0}^{G^-,L}P_L + C_{\Sigma^-\Sigma^0}^{G^-,R}P_R)\Sigma^0\} \\
&\quad + h.c
\end{aligned} \tag{B11}
$$

The exact vertex factors $C_{FI}^{X,L/R}$ for our two Higgs doublet Type III seesaw model are listed in Tables 9, 10, 11.

B.2 Lepton-Gauge coupling

The lepton-gauge couplings come from the kinetic energy terms for the Σ fields in the Lagrangian. The kinetic energy terms are given as

$$
-\mathcal{L}_k = \overline{\Sigma_R'} i\gamma^\mu D_\mu \Sigma_R{}' + L_k^{SM}, \tag{B12}
$$

$C^{H^0,L}_{\nu\nu}$	$\frac{\sin\alpha}{2}(U^T_{21}Y_\Sigma U_{11})$	$C^{H^0,R}_{\nu\nu}$	$\frac{\sin\alpha}{2}(U^\dagger_{11}Y^\dagger_\Sigma U^*_{21})$
$C^{H^0,L}_{\nu\Sigma^0}$	$\frac{\sin\alpha}{2}(U^T_{21}Y_\Sigma U_{12})$	$C^{H^0,R}_{\nu\Sigma^0}$	$\frac{\sin\alpha}{2}(U^\dagger_{11}Y^\dagger_\Sigma U^*_{22})$
$C^{H^0,L}_{\Sigma^0\Sigma^0}$	$\frac{\sin\alpha}{2}(U^T_{22}Y_\Sigma U_{12})$	$C^{H^0,R}_{\nu\Sigma^0}$	$\frac{\sin\alpha}{2}(U^\dagger_{12}Y^\dagger_\Sigma U^*_{22})$
$C^{h^0,L}_{\nu\nu}$	$\frac{\cos\alpha}{2}(U^T_{21}Y_\Sigma U_{11})$	$C^{h^0,R}_{\nu\nu}$	$\frac{\cos\alpha}{2}(U^\dagger_{11}Y^\dagger_\Sigma U^*_{21})$
$C^{h^0,L}_{\nu\Sigma^0}$	$\frac{\cos\alpha}{2}(U^T_{21}Y_\Sigma U_{12})$	$C^{h^0,L}_{\nu\Sigma^0}$	$\frac{\cos\alpha}{2}(U^\dagger_{11}Y^\dagger_\Sigma U^*_{22})$
$C^{h^0,L}_{\Sigma^0\Sigma^0}$	$\frac{\cos\alpha}{2}(U^T_{22}Y_\Sigma U_{12})$	$C^{h^0,R}_{\Sigma^0\Sigma^0}$	$\frac{\cos\alpha}{2}(U^\dagger_{12}Y^\dagger_\Sigma U^*_{22})$
$C^{A^0,L}_{\nu\nu}$	$\frac{i\cos\beta}{2}(U^T_{21}Y_\Sigma U_{11})$	$C^{A^0,R}_{\nu\nu}$	$-\frac{i\cos\beta}{2}(U^\dagger_{11}Y^\dagger_\Sigma U^*_{21})$
$C^{A^0,L}_{\nu\Sigma^0}$	$\frac{i\cos\beta}{2}(U^T_{21}Y_\Sigma U_{12})$	$C^{A^0,R}_{\nu\Sigma^0}$	$-\frac{i\cos\beta}{2}(U^\dagger_{11}Y^\dagger_\Sigma U^*_{22})$
$C^{A^0,L}_{\Sigma^0\Sigma^0}$	$\frac{i\cos\beta}{2}(U^T_{22}Y_\Sigma U_{12})$	$C^{A^0,R}_{\Sigma^0\Sigma^0}$	$-\frac{i\cos\beta}{2}(U^\dagger_{12}Y^\dagger_\Sigma U^*_{22})$
$C^{G^0,L}_{\nu\nu}$	$\frac{i\sin\beta}{2}(U^T_{21}Y_\Sigma U_{11})$	$C^{G^0,R}_{\nu\nu}$	$-\frac{i\sin\beta}{2}(U^\dagger_{11}Y^\dagger_\Sigma U^*_{21})$
$C^{G^0,L}_{\nu\Sigma^0}$	$\frac{i\sin\beta}{2}(U^T_{21}Y_\Sigma U_{12})$	$C^{G^0,R}_{\nu\Sigma^0}$	$-\frac{i\sin\beta}{2}(U^\dagger_{11}Y^\dagger_\Sigma U^*_{22})$
$C^{G^0,L}_{\Sigma^0\Sigma^0}$	$\frac{i\sin\beta}{2}(U^T_{22}Y_\Sigma U_{12})$	$C^{G^0,R}_{\Sigma^0\Sigma^0}$	$-\frac{i\sin\beta}{2}(U^\dagger_{12}Y^\dagger_\Sigma U^*_{22})$

Table 10: The vertex factors for P_L (P_R) and their corresponding exact expression in terms of the Yukawa couplings and mixing matrices are given in the first (third) and second (forth) column respectively. The vertex factors listed here are for Yukawa interactions of the neutral leptons with neutral Higgs.

$C^{H^-,L}_{l\nu}$	$-T^\dagger_{11}Y_l U_{11}\sin\beta$	$C^{H^-,R}_{l\nu}$	$(\frac{1}{\sqrt{2}}S^\dagger_{11}Y^\dagger_\Sigma {U_{21}}^* - S^\dagger_{21}{Y_\Sigma}^* {U_{11}}^*)\cos\beta$
$C^{H^-,L}_{l\Sigma^0}$	$-T^\dagger_{11}Y_l U_{12}\sin\beta$	$C^{H^-,R}_{l\Sigma^0}$	$(\frac{1}{\sqrt{2}}S^\dagger_{11}Y^\dagger_\Sigma {U_{22}}^* - S^\dagger_{21}{Y_\Sigma}^* {U_{12}}^*)\cos\beta$
$C^{H^-,L}_{\nu\Sigma^-}$	$(\frac{1}{\sqrt{2}}U^T_{21}Y_\Sigma S_{12} - U^T_{11}{Y_\Sigma}^T S_{22})\cos\beta$	$C^{H^-,R}_{\Sigma^-\nu}$	$-U^\dagger_{11}{Y_l}^\dagger T_{12}\sin\beta$
$C^{H^-,L}_{\Sigma^-\Sigma^0}$	$-T^\dagger_{12}Y_l U_{12}\sin\beta$	$C^{H^-,R}_{\Sigma^-\Sigma^0}$	$(\frac{1}{\sqrt{2}}S^\dagger_{12}Y^\dagger_\Sigma {U_{22}}^* - S^\dagger_{22}{Y_\Sigma}^* {U_{12}}^*)\cos\beta$
$C^{G^-,L}_{l\nu}$	$T^\dagger_{11}Y_l U_{11}\cos\beta$	$C^{G^-,R}_{l\nu}$	$(\frac{1}{\sqrt{2}}S^\dagger_{11}Y^\dagger_\Sigma {U_{21}}^* - S^\dagger_{21}{Y_\Sigma}^* {U_{11}}^*)\sin\beta$
$C^{G^-,L}_{l\Sigma^0}$	$T^\dagger_{11}Y_l U_{12}\cos\beta$	$C^{G^-,R}_{l\Sigma^0}$	$(\frac{1}{\sqrt{2}}S^\dagger_{11}Y^\dagger_\Sigma {U_{22}}^* - S^\dagger_{21}{Y_\Sigma}^* {U_{12}}^*)\sin\beta$
$C^{G^-,L}_{\nu\Sigma^-}$	$(\frac{1}{\sqrt{2}}U^T_{21}Y_\Sigma S_{12} - U^T_{11}{Y_\Sigma}^T S_{22})\sin\beta$	$C^{G^-,R}_{\Sigma^-\nu}$	$U^\dagger_{11}{Y_l}^\dagger T_{12}\cos\beta$
$C^{G^-,L}_{\Sigma^-\Sigma^0}$	$T^\dagger_{12}Y_l U_{12}\cos\beta$	$C^{G^-,R}_{\Sigma^-\Sigma^0}$	$(\frac{1}{\sqrt{2}}S^\dagger_{12}Y^\dagger_\Sigma {U_{22}}^* - S^\dagger_{22}{Y_\Sigma}^* {U_{12}}^*)\sin\beta$

Table 11: The vertex factors for P_L (P_R) and their corresponding exact expression in terms of the Yukawa couplings and mixing matrices are given in the first (third) and second (forth) column respectively. The vertex factors listed here are for Yukawa interactions of the charged as well as neutral leptons with charged Higgs.

where the first term is for heavy triplet fermion field and the second term contains the corresponding contributions from all standard model fields. The Σ'_R field is defined in Eq. (5). The covariant derivative is defined as

$$D_\mu = \partial_\mu - \sqrt{2}g \begin{pmatrix} W_\mu^3 & W_\mu^+ \\ W_\mu^- & -W_\mu^3 \end{pmatrix}. \tag{B13}$$

Inserting the covariant derivative in Eq. (B12) one obtains the following interaction terms between leptons and gauge fields

$$\mathcal{L}_{int} = \mathcal{L}_{NC}^{l,\Sigma^-} + \mathcal{L}_{NC}^{\nu,\Sigma^0} + \mathcal{L}_{CC}, \tag{B14}$$

where the first two terms contain the neutral current interactions between $l^\pm$ and $\Sigma^\pm$ (first term) and between ν and Σ^0 (second term) respectively. The last term gives the charged current interaction between the leptons. The neutral current interaction Lagrangian involving l and Σ^- is given by

$$\begin{aligned} \mathcal{L}_{NC}^{l,\Sigma^-} &= \overline{l}\gamma^\mu\{c_{ll}^{Z,R}P_R + c_{ll}^{Z,L}P_L\}l\, Z_\mu + \{\overline{l}\gamma^\mu\{c_{l\Sigma^-}^{Z,R}P_R + c_{l\Sigma^-}^{Z,L}P_L\}\Sigma^- Z_\mu + h.c\} \\ &\quad + \overline{\Sigma^-}\gamma^\mu\{c_{\Sigma^-\Sigma^-}^{Z,R}P_R + c_{\Sigma^-\Sigma^-}^{Z,L}P_L\}\Sigma^- Z_\mu, \end{aligned} \tag{B15}$$

where

$$\begin{aligned} c_{ll}^{Z,R} &= \frac{g}{c_w}s_w^2(T_{11}^\dagger T_{11}) - c_w g(T_{21}^\dagger T_{21})\}, \\ c_{l\Sigma^-}^{Z,R} &= \frac{g}{c_w}s_w^2(T_{11}^\dagger T_{12}) - c_w g(T_{21}^\dagger T_{22}), \\ c_{\Sigma^-\Sigma^-}^{Z,R} &= \frac{g}{c_w}s_w^2(T_{12}^\dagger T_{12}) - c_w g(T_{22}^\dagger T_{22}), \end{aligned} \tag{B16}$$

$$\begin{aligned} c_{ll}^{Z,L} &= \frac{g}{c_w}(-\frac{1}{2} + s_w^2)(S_{11}^\dagger S_{11}) - c_w g(S_{21}^\dagger S_{21}), \\ c_{l\Sigma^-}^{Z,L} &= \frac{g}{c_w}(-\frac{1}{2} + s_w^2)(S_{11}^\dagger S_{12}) - c_w g(S_{21}^\dagger S_{22}), \\ c_{\Sigma^-\Sigma^-}^{Z,L} &= \frac{g}{c_w}(-\frac{1}{2} + s_w^2)(S_{12}^\dagger S_{12}) - c_w g(S_{22}^\dagger S_{22}). \end{aligned} \tag{B17}$$

The neutral current interaction Lagrangian involving the neutral leptons is given by

$$\begin{aligned} \mathcal{L}_{NC}^{\nu,\Sigma^0} &= (gc_w + g's_w)\frac{1}{2}\overline{\nu}\gamma^\mu\{(U_{11}^\dagger U_{11})P_L\}\nu Z_\mu \\ &\quad + (gc_w + g's_w)\frac{1}{2}\overline{\Sigma^0}\gamma^\mu\{(U_{12}^\dagger U_{12})P_L\}\Sigma^0 Z_\mu \\ &\quad + \{(gc_w + g's_w)\frac{1}{2}\overline{\nu}\gamma^\mu\{(U_{11}^\dagger U_{12})P_L\}\Sigma^0 Z_\mu + \text{h.c}\}. \end{aligned} \tag{B18}$$

The charged current interaction Lagrangian is given by

$$\begin{aligned}\mathcal{L}_{CC} &= g\overline{\nu}\gamma^{\mu}\{\{(U_{21}^{\dagger}S_{21})+\frac{1}{\sqrt{2}}(U_{11}^{\dagger}S_{11})\}P_L+(U_{21}^{T}T_{21})P_R\}lW_{\mu}^{+} \\ &+g\overline{\nu}\gamma^{\mu}\{\{(U_{21}^{\dagger}S_{22})+\frac{1}{\sqrt{2}}(U_{11}^{\dagger}S_{12})\}P_L+(U_{21}^{T}T_{22})P_R\}\Sigma^{-}W_{\mu}^{+} \\ &+g\overline{\Sigma^0}\gamma^{\mu}\{\{(U_{22}^{\dagger}S_{21})+\frac{1}{\sqrt{2}}(U_{12}^{\dagger}S_{11})\}P_L+(U_{22}^{T}T_{21})P_R\}lW_{\mu}^{+} \\ &+g\overline{\Sigma^0}\gamma^{\mu}\{\{(U_{22}^{\dagger}S_{22})+\frac{1}{\sqrt{2}}(U_{12}^{\dagger}S_{12})\}P_L+(U_{22}^{T}T_{22})P_R\}\Sigma^{-}W_{\mu}^{+}+h.c\end{aligned} \tag{B19}$$

B.3 Quark-Higgs coupling

Finally, we discuss the the Yukawa Lagrangian for quark sector, which is given by

$$-\mathcal{L}_Q = Y_{U_{ij}}\overline{u'_{R_i}}\tilde{\Phi}_1^{\dagger}Q'_j+Y_{D_{ij}}\overline{d'_{R_i}}\Phi_1^{\dagger}Q'_j+h.c, \tag{B20}$$

where Q' is the left-handed quark doublet and u'_R and d'_R are the right-handed "up" and "down" types of quark fields. Again, primes denote the flavor bases. After the electroweak spontaneous symmetry breaking the up and down quark mass matrices are obtained as

$$\begin{aligned}M_U &= Y_U v \\ M_D &= Y_D v\end{aligned} \tag{B21}$$

Note that only Φ_1 couples to both the up and down quark fields due to the imposed Z_2 symmetry, while the Yukawa couplings of Φ_2 to quarks is forbidden[10]. However, due to the mixing between Higgs fields as discussed in Appendix A, all the physical Higgs particles would couple to the quark fields. Here we list all the interaction vertices between quarks and Higgs fields, which are specific to our model. The fields represents the fields in the mass basis.

$$-\mathcal{L}_{u,d}^{H^0} = \frac{1}{\sqrt{2}}\frac{cos\alpha}{v}\overline{u}M_u u H^0+\frac{1}{\sqrt{2}}\frac{cos\alpha}{v}\overline{d}M_d d H^0 \tag{B22}$$

$$-\mathcal{L}_{u,d}^{h^0} = -\frac{1}{\sqrt{2}}\frac{sin\alpha}{v}\overline{u}M_u u h^0-\frac{1}{\sqrt{2}}\frac{sin\alpha}{v}\overline{d}M_d d h^0 \tag{B23}$$

$$-\mathcal{L}_{u,d}^{A^0} = i\frac{1}{\sqrt{2}}\frac{sin\beta}{v}\overline{u}\gamma^5 M_u u A^0-i\frac{1}{\sqrt{2}}\frac{sin\beta}{v}\overline{d}\gamma^5 M_d d A^0 \tag{B24}$$

[10]This is a major difference between our model and other two Higgs doublet models where the Higgs which couples to the neutrinos also couples to the up type quarks, while the one which couples to the charged leptons couples to the down type quarks.

$$-\mathcal{L}_{u,d}^{G^0} = -i\frac{1}{\sqrt{2}}\frac{cos\beta}{v}\overline{u}\gamma^5 M_u u G^0 + i\frac{1}{\sqrt{2}}\frac{cos\beta}{v}\overline{d}\gamma^5 M_d d G^0 \quad \text{(B25)}$$

$$-\mathcal{L}_{u,d}^{G^\pm} = \frac{cos\beta}{v}\overline{u}(V_{CKM}M_d P_R - M_u V_{CKM} P_L)d + h.c \quad \text{(B26)}$$

$$-\mathcal{L}_{u,d}^{H^\pm} = -\frac{sin\beta}{v}\overline{u}(V_{CKM}M_d P_R - M_u V_{CKM} P_L)d + h.c \quad \text{(B27)}$$

References

[1] P. Minkowski, Phys. Lett. B **67**, 421 (1977); M. Gell-Mann, P. Ramond, and R. Slansky, *Supergravity* (P. van Nieuwenhuizen et al. eds.), North Holland, Amsterdam, 1980, p. 315; T. Yanagida, in *Proceedings of the Workshop on the Unified Theory and the Baryon Number in the Universe* (O. Sawada and A. Sugamoto, eds.), KEK, Tsukuba, Japan, 1979, p. 95; S. L. Glashow, *The future of elementary particle physics*, in *Proceedings of the 1979 Cargèse Summer Institute on Quarks and Leptons* (M. Lévy et al. eds.), Plenum Press, New York, 1980, pp. 687; R. N. Mohapatra and G. Senjanović, Phys. Rev. Lett. **44**, 912 (1980).

[2] S. Weinberg, Phys. Rev. Lett. **43**, 1566 (1979).

[3] M. Magg and C. Wetterich, Phys. Lett. B **94**, 61 (1980); J. Schechter and J. W. F. Valle, Phys. Rev. D **22**, 2227 (1980); C. Wetterich, Nucl. Phys. B **187**, 343 (1981); G. Lazarides, Q. Shafi and C. Wetterich, Nucl. Phys. B **181**, 287 (1981); R. N. Mohapatra and G. Senjanovic, Phys. Rev. D **23**, 165 (1981).

[4] R. Foot, H. Lew, X. G. He and G. C. Joshi, Z. Phys. C **44**, 441 (1989).

[5] E. Ma, Phys. Rev. Lett. **81**, 1171 (1998) [arXiv:hep-ph/9805219].

[6] E. Ma and D. P. Roy, Nucl. Phys. B **644**, 290 (2002) [arXiv:hep-ph/0206150]; R. Adhikari, J. Erler and E. Ma, Phys. Lett. B **672**, 136 (2009) [arXiv:0810.5547 [hep-ph]].

[7] T. Hambye, Y. Lin, A. Notari, M. Papucci and A. Strumia, Nucl. Phys. B **695**, 169 (2004) [arXiv:hep-ph/0312203].

[8] P. Fileviez Perez, Phys. Lett. B **654**, 189 (2007) [arXiv:hep-ph/0702287]; P. Fileviez Perez, Phys. Rev. D **76**, 071701 (2007) [arXiv:0705.3589 [hep-ph]].

[9] R. N. Mohapatra, N. Okada and H. B. Yu, Phys. Rev. D **78**, 075011 (2008) [arXiv:0807.4524 [hep-ph]].

[10] P. Fileviez Perez, JHEP **0903**, 142 (2009) [arXiv:0809.1202 [hep-ph]].

[11] I. Gogoladze, N. Okada and Q. Shafi, Phys. Lett. B **668**, 121 (2008) [arXiv:0805.2129 [hep-ph]].

[12] J. Chakrabortty, A. Dighe, S. Goswami and S. Ray, arXiv:0812.2776 [hep-ph].

[13] Y. Liao, J. Y. Liu and G. Z. Ning, Phys. Rev. D **79**, 073003 (2009) [arXiv:0902.1434 [hep-ph]].

[14] A. Abada, C. Biggio, F. Bonnet, M. B. Gavela and T. Hambye, JHEP **0712**, 061 (2007) [arXiv:0707.4058 [hep-ph]].

[15] A. Abada, C. Biggio, F. Bonnet, M. B. Gavela and T. Hambye, Phys. Rev. D **78**, 033007 (2008) [arXiv:0803.0481 [hep-ph]].

[16] A. Arhrib, R. Benbrik and C. H. Chen, arXiv:0903.1553 [hep-ph].

[17] B. Bajc and G. Senjanovic, JHEP **0708**, 014 (2007) [arXiv:hep-ph/0612029].

[18] B. Bajc, M. Nemevsek and G. Senjanovic, Phys. Rev. D **76**, 055011 (2007) [arXiv:hep-ph/0703080].

[19] R. Franceschini, T. Hambye and A. Strumia, Phys. Rev. D **78**, 033002 (2008) [arXiv:0805.1613 [hep-ph]].

[20] F. del Aguila and J. A. Aguilar-Saavedra, Nucl. Phys. B **813**, 22 (2009) [arXiv:0808.2468 [hep-ph]].

[21] A. Arhrib, B. Bajc, D. K. Ghosh, T. Han, G. Y. Huang, I. Puljak and G. Senjanovic, arXiv:0904.2390 [hep-ph].

[22] S. Gabriel and S. Nandi, Phys. Lett. B **655**, 141 (2007) [arXiv:hep-ph/0610253].

[23] *"THE HIGGS HUNTER'S GUIDE"*, J. F. Gunion, H. E. Haber, G. L. Kane and S. Dawson, Perseus Publishings, Massachusetts.

[24] D. Atwood, S. Bar-Shalom and A. Soni, Phys. Lett. B **635**, 112 (2006) [arXiv:hep-ph/0502234].

[25] S. Antusch, M. Drees, J. Kersten, M. Lindner and M. Ratz, Phys. Lett. B **525**, 130 (2002) [arXiv:hep-ph/0110366].

[26] K. Matsuda, Y. Koide, T. Fukuyama and H. Nishiura, Phys. Rev. D **65**, 033008 (2002) [Erratum-ibid. D **65**, 079904 (2002)] [arXiv:hep-ph/0108202].

[27] M. Aoki, S. Kanemura and O. Seto, arXiv:0904.3829 [hep-ph].

[28] T. Fukuyama and H. Nishiura, hep-ph/9702253; R. N. Mohapatra and S. Nussinov, Phys. Rev. D **60**, 013002 (1999); E. Ma and M. Raidal, Phys. Rev. Lett. **87**, 011802 (2001); C. S. Lam, Phys. Lett. B **507**, 214 (2001); P.F. Harrison and W. G. Scott, Phys. Lett. B **547**, 219 (2002); T. Kitabayashi and M. Yasue, Phys. Rev. D **67**, 015006 (2003); W. Grimus and L. Lavoura, Phys. Lett. B **572**, 189 (2003); J. Phys. G **30**, 73 (2004); Y. Koide, Phys. Rev. D **69**, 093001 (2004); A. Ghosal, hep-ph/0304090; W. Grimus *et al.*, Nucl. Phys. B **713**, 151 (2005); R. N. Mohapatra, JHEP **0410**, 027 (2004); A. de Gouvea, Phys. Rev. D **69**, 093007 (2004); R. N. Mohapatra and W. Rodejohann, Phys. Rev. D **72**, 053001 (2005); R. N. Mohapatra and S. Nasri, Phys. Rev. D **71**, 033001 (2005); R. N. Mohapatra, S. Nasri and H. B. Yu, Phys. Lett. B **615**, 231 (2005); Phys. Rev. D **72**, 033007 (2005); Y. H. Ahn*et al.*, Phys. Rev. D **73**, 093005 (2006); B. Brahmachari and S. Choubey, Phys. Lett. B **642**, 495 (2006); K. Fuki, M. Yasue, hep-ph/0608042. S. Choubey and W. Rodejohann, Eur. Phys. J. C **40**, 259 (2005).

[29] W. Grimus and L. Lavoura, JHEP **0011**, 042 (2000) [arXiv:hep-ph/0008179].

[30] M. Mitra and S. Choubey, Phys. Rev. D **78**, 115014 (2008) [arXiv:0806.3254 [hep-ph]].

[31] M. Maltoni, T. Schwetz, M. A. Tortola and J. W. F. Valle, New J. Phys. **6**, 122 (2004), hep-ph/0405172 v6; A. Bandyopadhyay, S. Choubey, S. Goswami, S. T. Petcov and D. P. Roy, arXiv:0804.4857 [hep-ph]. G. L. Fogli *et al.*, Phys. Rev. D **78**, 033010 (2008) [arXiv:0805.2517 [hep-ph]].

[32] H. L. Lai *et al.* [CTEQ Collaboration], Phys. Rev. D **55**, 1280 (1997) [arXiv:hep-ph/9606399]; http://projects.hepforge.org/lhapdf/

[33] See *"http://hep.pa.msu.edu/people/belyaev/public/calchep/index.html"* .

[34] G. Aad *et al.* [The ATLAS Collaboration], arXiv:0901.0512 [hep-ex].

[35] See the CMS Physics Technical Design Report (Volume I and II) at *http://cms.web.cern.ch/cms/Physics/index.html*

[36] G. Altarelli and F. Feruglio, Nucl. Phys. B **741**, 215 (2006); G. Altarelli , F. Feruglio and Y. Lin, Nucl. Phys. B **775**, 31 (2007).